Endothelial cells signaling and patterning under hypoxia: a mechanistic computational model

Rebeca Hannah M Oliveira[1], Brian H. Annex[2], Aleksander S. Popel[1]

[1]Department of Biomedical Engineering, School of Medicine, Johns Hopkins University, Baltimore, Maryland, 21205, USA

[2]Medical College of Georgia, Augusta University, Augusta, Georgia, USA

ABSTRACT

Several signaling pathways are activated during hypoxia to promote angiogenesis, leading to endothelial cell patterning, interaction, and downstream signaling. Understanding the mechanistic signaling differences between normoxia and hypoxia can guide therapies to modulate angiogenesis. We present a novel mechanistic model of interacting endothelial cells, including the main pathways involved in angiogenesis. We calibrate and fit the model parameters based on well-established modeling techniques. Our results indicate that the main pathways involved in the patterning of tip and stalk endothelial cells under hypoxia differ, and the time under hypoxia affects how a reaction affects patterning. Interestingly, the interaction of receptors with Neuropilin1 is also relevant for cell patterning. Our simulations under different oxygen concentrations indicate time- and oxygen-availability-dependent responses for the two cells. Following simulations with various stimuli, our model suggests that factors such as period under hypoxia and oxygen availability must be considered for pattern control. This project provides insights into the signaling and patterning of endothelial cells under hypoxia, contributing to studies in the field.

Keywords: angiogenesis, modeling, systems biology, hypoxia, endothelial cells

1. INTRODUCTION

The formation of new blood vessels from the existing vasculature, called angiogenesis, is regulated by different cells and events Carmeliet, 2005; Eelen et al., 2020; Zhang et al., 2022) . It is generally classified as sprouting angiogenesis (sprouting of endothelial cells from a mother vessel based on environmental cues) or intussusceptive angiogenesis (vessel splitting internally into two daughter vessels), with the former being better characterized and studied than the latter, and both essential for regeneration of microvasculature (Arpino et al., 2021). Dysregulation in angiogenesis has been associated with the development and complication of different diseases, such as cancer, diabetic retinopathy, age-related macular degeneration, and cardiovascular diseases, including peripheral arterial disease (PAD) (Zhang et al. 2021). Many studies focus on modulating and controlling angiogenesis as a therapeutic approach for treating

ischemic diseases and cancer (Annex and Cooke, 2021; Teleanu et al., 2019). PAD, for instance, is an atherosclerotic disease characterized by lower limb ischemia and where the greater the extent of the endogenous angiogenic response, the lesser the patients' symptoms. Often accompanied by severe microvascular disease, PAD affects more than 200 million people worldwide and is associated with 53–90% of all major amputations of the lower limb (Londero et al., 2019; Aday and Matsushita, 2021). Currently, there is no cure for this disease, and medical therapies have limited efficacy in treating it. Therapeutic angiogenesis remains a approach that hopes to alter the course of the disease (Annex and Cooke, 2021; Han et al., 2022). Among the main signaling pathways that regulate angiogenesis are the Notch signaling and the oxygen sensing hypoxia-inducible factor (HIF) pathways. Under hypoxia, VEGFA (and possibly other angiogenic factors) is released in the hypoxic tissue, guiding ECs to the ischemic site to restore blood flow and oxygen availability. Once attracted, ECs compete for the tip position, a dynamic process guided by the Notch signaling pathway and affected by hypoxia (Figure 1) (Naito et al., 2020).

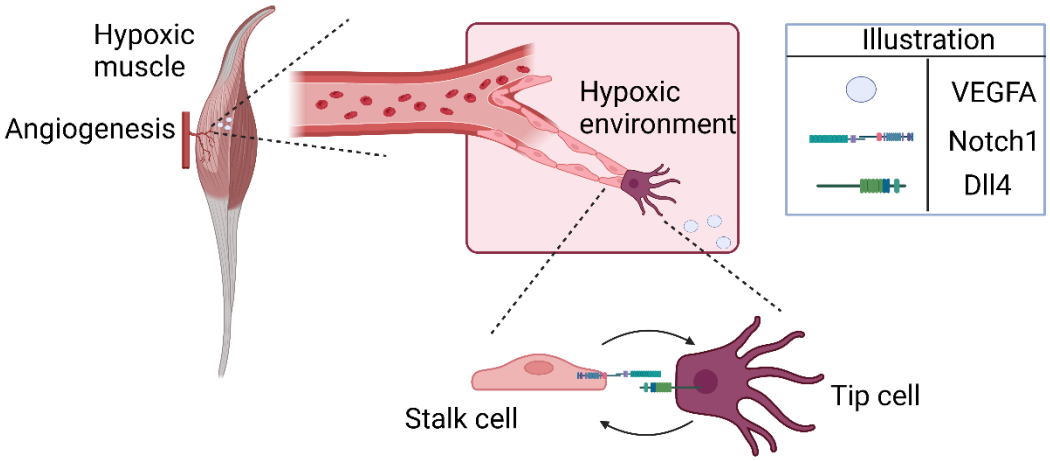

Figure 1: Hypoxia-induced cell patterning during angiogenesis (illustrated here for the specific example of ischemic skeletal muscle). Endothelial cells approach the hypoxic region, attracted by higher concentrations of VEGFA. The cells interact through Notch1-Dll4, competing for the tip position.

The Notch signaling pathway is a major regulator of cell fate, cell differentiation, vascular patterning, and intercellular communication in processes such as angiogenesis and tumor growth. The Notch pathway is highly conserved across vertebrates, and it affects different cells, such as macrophages, endothelial cells (ECs), smooth muscle cells (SMCs), and pericytes (Akil et al., 2021). During sprouting angiogenesis, the extracellular Notch ligands (Jagged 1, 2; Delta-like ligands 1, 3, and 4) initiate the signaling by interacting with Notch receptors (Notch 1-4) on the surface of ECs. Once the binding occurs, a series of proteolytic events occur, mediated by disintegrin metalloproteinase domain-containing protein 10 (ADAM10) and the $\gamma_{secretase}$ enzymes.

$\gamma_{secretase}$ cleaves the surface of the Notch receptor intracellular domain (NICD), releasing it in the cell cytoplasm. NICD translocates to the nucleus, where it binds to the recombination of signal-binding protein for the immunoglobulin kappa J region (RBPJ). The complex acts as a transcriptional activator, promoting the transcription of Notch target genes such as transcriptional repressors Hairy Enhancer of Split (Hes) and Hes-related with YRPW motif (HEY1) genes. These genes regulate EC patterning and tip EC formation, migration, and proliferation, to promote functional angiogenesis (Swaminathan et al., 2022). In EC differentiation, Delta-like ligand 4 (Dll4) and Jagged 1 present different effects when interacting with Notch receptors. While Dll4 is a negative regulator of tip cell formation, Jagged 1 positively regulates tip cell formation and sprouting (Benedito et al., 2009; Pedrosa et al., 2015). Dll4 and Jagged also have a role on spatial control of sprouting (Tiemeijer et al., 2022). This competition between Notch ligands to bind to the Notch receptor is required to promote functional revascularization and tissue reperfusion.

Different cells in ischemic tissues release pro-angiogenic factors such as vascular endothelial growth factor (VEGF) (Couffinhal et al., 1998; Rissanen et al., 2002). VEGF induces endothelial cell migration and sprouting in a chemotaxis-dependent fashion (Lee et al., 2022). This pro-angiogenesis mechanism depends on environmental cues such as low oxygen levels, driven by the HIF signaling pathway. Once low oxygen levels are sensed in the tissue, three types of hypoxia-inducible factors (HIF-1, HIF-2, HIF-3), are activated, each composed of two subunits (α and β). The α-subunits are regulated by changes in oxygen concentration based on proteolytic degradation and transcriptional regulation. In normoxic conditions, HIF1-α is hydroxylated on its proline residue by different isoforms of prolyl hydroxylase (PHD), and sequentially ubiquitinated by von Hippel-Lindau protein (pVHL). Finally, HIF1-α undergoes proteasomal degradation. The enzyme factor inhibiting HIF (FIH) also regulates the transcriptional activity of HIF1-α through hydroxylation of asparagine residues, which inhibits the interaction between HIF1-α subunit and CBP/p300, an interaction required for the transcription of HIF-dependent genes. However, under low oxygen concentrations, both FIH and PHD activities are reduced, and the hydroxylation of HIF-α does not occur. In this case, HIF1-α becomes more stable and translocates to the nucleus, where it dimerizes with HIF1-β. The newly-formed complex then bonds to the hypoxia element site on DNA, leading to the expression of different genes as a response to hypoxia, along with VEGF, erythropoietin (EPO), and glycolytic enzymes (Korbecki et al., 2021; Zhang et al., 2018). Under ischemia, HIF1-α upregulation relates to tissue inflammation, and it has been an important therapeutic target and molecule of interest in angiogenesis models (Qutub & Popel, 2006, 2007, 2008).

The HIF pathway and the Notch pathway are essential in the response to ischemia and understanding the mechanistic interactions between them and other pathways that drive EC differentiation, proliferation and stability can help in the development of new therapeutic strategies for diseases such as PAD. Even for converging pathways, differences in temporal regulation affect their signaling outcomes (Jin et al., 2014). Computational models have been developed and provided important insights into the understanding of signaling pathways and

cell-cell interactions (Subramanian et al., 2022). For instance, Zhao et al. designed an ODE (ordinary differential equation)-based computational model to understand hypoxia-responsive miRNAs control of the HIF-VEGF pathway in EC (Zhao and Popel, 2015). Also, Venkatraman et al. formulated an ODE-based mathematical model to better understand how local and intracellular conditions influence EC patterning (tip or stalk EC) (Venkatraman et al., 2016). Their model showed a partial and stable tip/stalk stage with duration determined by intracellular signaling.

To date, most computational models of endothelial cell patterning during angiogenesis are based on Cellular Pots or agent-based modeling strategies (Kühn and Checa, 2019). Previous agent-based models on the Notch signaling report how VEGF concentration relates to elongation, migration and proliferation of ECs (Qutub & Popel, 2009). Recently, Koon and colleagues presented a computational model of EC patterning focusing on Notch signaling heterogeneity to explain a greater variety of cell patterning. They report hybrid endothelial cells with both tip and stalk characteristics (Koon et al., 2018). A more comprehensive Boolean model including different signaling pathways in EC during angiogenesis was presented by Weinstein et al., incorporating the molecular regulatory network, extracellular micro-environments and loss- and gain-of-function mutations (Weinstein et al., 2017). Mechanistic models of signaling networks in EC have also been developed. Bazzazi et al. designed a rule-based computational model to assess the effects of thrombospondin-1 (TSP1)-CD47 signaling through VEGF on ERK1/2 and calcium (Bazzazi et al., 2017). The group also investigated TSP1 inhibition of VEGF signaling to Akt-endothelial nitric oxide synthase (eNOS) using rule-based modeling (Bazzazi et al., 2018). A hybrid multi-scale model of endothelial cells during angiogenesis has also been presented by Stepanova et al., including features such as branching, cell mixing, and the brush border effect. Their work indicated a dependence on the time evolution of cell mixing and the newly formed branching structure (Stepanova et al., 2021).

The complex molecular signaling networks that drive angiogenesis and determine EC fate are largely affected by hypoxia; note that the effect may be context-dependent and differ in different tissues such as ischemic skeletal muscle, tumor, or ischemic retina. External stimulation through VEGF and signaling between interacting ECs determine cell fate and guide downstream signaling, contributing to functional angiogenesis. In this work, we assess changes in the dynamics of such networks under hypoxia conditions, to understand how VEGF, Notch, and HIF signaling pathways interact with each other and regulate downstream pathways, as well as how they affect EC patterns through time. Using a mechanistic model of two interacting ECs, we evaluate their signal exchange under varying oxygen conditions, investigate the effects of different interventions on cell pattern determination and discuss their potential application in the context of angiogenesis modulation.

2. Methods

We formulate the model network based on biological knowledge and experimental evidence and obtain the corresponding ordinary differential equations representing each biochemical reaction. The reactions are based on mass action, Hill, and Michaelis Menten kinetics. The model is implemented in the Matlab SimBiology software. The final model comprises 224 species, 251 reactions, and 200 parameters. The sbml. and Matlab files are provided as supplementary material (tables S2-S4), with the initial conditions and parameter values used. A description of model components is also provided. The model was simulated using MATLAB R2022a (MathWorks, Natick, MA, United States) with ode15s as the ODE solver. Considering the numerous effects of hypoxia on angiogenesis-involved signaling pathways (Rodriguez et al., 2021), we model the ones considered more relevant to our understanding of the interaction between ECs. They are listed in table 1.

Table 1. The effects of hypoxia in endothelial cells included in the model.

Effects of hypoxia on Endothelial Cells	
Upregulates	Downregulates
Dll4, Hes1	VEGFR2
VEGFA, VEGFR1	Akt phosphorylation
Calcium in cytosol	eNOS phosphorylation

2.1. Model parameterization

Our first step in model parameterization focused on an a priori identifiability analysis of the model. Structural identifiability investigates the possibility of obtaining a unique value for each parameter in a model considering a known and theoretically perfect model structure. It allows us to select which parameters can be considered for fitting. Several methods are available for performing this analysis, as recently reviewed (Rey Barreiro & Villaverde, 2023). Due to Matlab compatibility, we used GenSSI to perform this analysis (Chiş et al., 2011; Ligon et al., 2018). Non-identifiable parameters were not included in the fitting process. Unknown parameter values were assumed.

Following the analysis, we used hand-tuning followed by Particle Swarm Optimization method (Iadevaia et al., 2010) to fit the model structural globally identifiable parameters to experimental data, with the built-in sbiofit function for SimBiology models. For the fitting, we obtained data from Western blots and densitometric data available in the literature for endothelial cells, using ImageJ to quantify Western blot data (Schneider et al., 2012). We apply the Runs test on calculated residuals to assess goodness of fit, as described in Motulsky and Ransnas (1987). We also obtained the 95% Gaussian confidence intervals (included as supplementary material). While some parameter values and species initial concentrations were obtained/adapted from previous

computational models (Bazzazi et al., 2017, 2018; Venkatraman et al., 2016; Zhao & Popel, 2015), some were estimated (hand-tuned) to improve fitting.

2.2. Sensitivity analysis and endothelial cell pattern index

We used PRCC to perform a global sensitivity analysis, based on the program from Renardy et al. (2019), evaluating the sensitivity at four time points (1 hour, 2 hours, 10 hours, and 24 hours). For graphical illustration, we calculated the average PRCC values corresponding to p-values less than 0.05. In this work, we define the endothelial cell pattern index (ECPI) as a ratio that identifies the cell as tip or stalk based on its expression of Dll4, VEGFR2, and Hes1 proteins. We use the ECPI to quantify the relative changes within the tip-stalk pattern over time. The ECPI is calculated by

$$\mathrm{ECPI} = \frac{[\mathrm{VEGFR2}] * [\mathrm{Dll4}]}{1 + [\mathrm{Hes1}]},$$

where $[\mathrm{x}]$ represents the molar concentration of a species. Since the initial concentration of Hes1 in our model is zero, we add one to the denominator to compute the ratio. We performed the sensitivity calculations with ECPI as the output for previously stated time points. The results are presented in Figure 5 and Supplementary Table S1. Additionally, to investigate the influence of VEGFR2 initial values on cell patterning, we performed local sensitivity analysis scanning over a range of values of VEGFR2 in both cells. The results are reported in Figure S4.

3. SIGNALING PATHWAYS DESCRIPTION

In this section, we detail the signaling pathways included in the model and how they intersect.

3.1. The VEGF-VEGFR2 signaling pathway

In a hypoxic environment, VEGF is released to induce angiogenesis and normalize oxygen levels. Tip endothelial cells probe the environment with their filopodia protrusions and migrate to the site of higher VEGF concentration, where the ligands bind to VEGF receptors located on the cell's surface. VEGF can bind to VEGFR2, VEGFR1, or neuropilin-1 (NRP1), forming complexes with different reaction rates and binding affinities. The interaction with VEGFR2 leads to its

205 phosphorylation. In the model, we also represent the internalization of free and bound VEGR2.
206 The internalized receptors can be degraded or recycled to the surface. Our simulations show a
207 more robust signal by internalized phosphorylated VEGFR2 (ipVR2) than surface phosphorylated
208 VEGFR2 (pR2). This agrees with previous models and experimental data (Bazzazi et al., 2017;
209 Weddell and Imoukhuede, 2017). This signaling pathway is shown in Figure 2A. Additionally, we
210 model the repression of VEGFR2 and stimulation of VEGFR1 by the Notch signaling pathway
211 (Figure 2C).

212

213 ## 3.2. The Notch signaling pathway

214

215 The Notch signaling pathway is shown in Figure 2C. In our model, we represent VEGFR2
216 phosphorylation as an inducer of Dll4 in both cells. Under hypoxia, the expression of Dll4 is also
217 noted. Dll4 of each cell binds to the Notch1 surface receptor of the other cell, initiating the Notch
218 signaling pathway. This interaction leads to cleavage of the NICD by $\gamma_{secretase}$

219 on the cell membrane. The cleaved domain translocates to the nucleus, binds to RBPJ (omitted
220 in the model for simplification), and upregulates the expression of Hes-1. Hes-1 downregulates
221 the surface VEGFR2 expression. We also represent VEGFR1 upregulation by Notch signaling,
222 considering this as a consequence of Hes1 transcription. Our model considers that Dll4, NICD,
223 Notch1 and Hes1 undergo degradation at different rates, fitted to experimental data.

224 Previous studies show that Notch signaling is modulated by the PI3K-Akt signaling through
225 modulation of $\gamma_{secretase}$ activity. Here, we consider that the oxygen-sensing module mediates this
226 interaction. Upon activation of the PI3K-Akt-mTORC1 pathway, mTORC1 leads to the formation
227 of HIF1-α in the cytoplasm. HIF1-α can then bind to $\gamma_{secretase}$, activating the enzyme. Activated
228 $\gamma_{secretase}$ will move on to perform its action on NICD. This model assumption is based on the
229 experimental work of (Villa et al., 2014).

230

231 ## 3.3. The Akt-mTORC1 signaling pathway

232

233 The Akt-eNOS-mTORC1 signaling pathway is shown in Figure 2B. The pathway is initiated by
234 VEGFR2 phosphorylation (surface and internalized). Phosphorylated VEGFR2 leads to the
235 activation of Src in a complex with TSAD. Following, Axl-1 is phosphorylated by phosphorylated
236 TSAD-Src and then undergoes a second auto-phosphorylation. The double-phosphorylated Axl-1
237 is recruited to the membrane and it activates PI3K. Following this, PI3K leads to the
238 phosphorylation of PIP2 to form PIP3 (a process that PTEN can reverse). PIP3 then recruits Akt
239 and PDK1 to the cell membrane. Following, mTORC2 kinase acts on recruited Akt, leading to its
240 phosphorylation on serine 473 residue. Then, the recruited PDK1 phosphorylates Akt on its
241 threonine 308 residue.

Phosphorylated Akt and phosphorylated ERK inhibit TSC2, a Rheb GTPase inhibitor. Therefore, pAkt and pERK promote RHEB-GTP complex formation, activating mTORC1 (Memmott and Dennis, 2009; Winter et al., 2011). In our model, these reactions are lumped together in a single reaction showing the activation of inactive mTORC1 by phosphorylated Akt and ERK.

3.4. The Oxygen sensing signaling pathway

The oxygen sensing pathway is represented in Figure 2D. Our model considers that HIF1-α is formed given the stimulus of mTORC1 activated by pAkt and pERK. Under normoxia, oxygen molecules form complexes with Fe-FIH-DG and Fe-DG-PHD2, leading to complex hydroxylation and subsequent polyubiquitination by VHL (von Hippel-Lindau ubiquitin E3 ligase), which marks them for degradation (Zhao and Popel, 2015; Hashimoto and Shibasaki, 2015). Under hypoxia, HIF1-α is stabilized and moves to the nucleus, where it dimerizes with HIF1-β. Intermediate steps, such as binding to CBP/p300, are lumped in the dimerization reaction of our model. The complex formed stimulates the production of VEGF, which increases the angiogenic response, and TTP (tristetraprolin), which inhibits HIF1-α in a negative feedback control (Kim et al., 2010; Chamboredon et al., 2011). For simplification, we do not include in our model the positive correlation between TTP and HIF1-α suggested by Fähling et al. (2012). Additionally, we do not model the effects of reactive oxygen species interaction with HIF1-α since it is not strictly relevant for this research focus. We assume PHD2 concentration to be in excess so that the feedback HIF/PHD can be disregarded, similar to the assumption made in the model of Zhao and Popel (2015).

3.5. The Raf-MEK-ERK signaling pathway

The phosphorylation of VEGFR2 also activates the Raf-MEK-ERK pathway, as shown in Figure 2F. In this pathway, PLC-γ is activated by pVEGFR2 and leads to the generation of DAG and IP3. DAG binds to PKC and calcium, leading to a sequence of activations and phosphorylation of Raf, MEK, ERK, and sphingosine kinase 1 (SphK). Activated IP3 stimulates calcium release from the endoplasmic reticulum, and the released calcium can bind to calcium and integrin binding protein 1 (CIB), forming a complex. Active SphK (pSphK) is translocated to the plasma membrane by CIB, and a complex is formed between will Ca-CIB-pSphK. SphK1 will then phosphorylate its ligand (Sph), forming diffusible sphingosine 1 phosphate (S1P). Finally, S1P activates Ras forming RasGTP, which stimulates Raf phosphorylation.

3.6. The Calcium cycling and eNOS phosphorylation pathway

IP3 activation by phosphorylated pVEGFR2 is one mechanism that controls the calcium cycling dynamics. Figure 2E represents this process, which relates to the phosphorylation of eNOS. Activated IP3 diffuses into the cell and binds to IP3 sensitive calcium release channels on the endoplasmic reticulum (ER). The binding leads to calcium release from the ER and a consequent decrease in calcium concentration in this compartment. This decrease causes calcium release-activated calcium channels (CRAC) to open, allowing extracellular calcium income. The action of surface membrane PM pump and ER SERCA channels balances calcium concentration in the cytosol.

Under hypoxia, we include in our model the activity of sodium-calcium exchanger ($Na^+ - Ca^{2+}$) proposed by Berna et al. (2002). Hypoxia inhibits mitochondrial oxidative phosphorylation, which increases the cellular requirement of glucose for anaerobic glycolysis to replenish energy. The required glucose can enter the cell via a Na^+-glucose-like co-transporter. The co-transporter increases the amount of Na^+ in the cytosol, which is then balanced by the $Na^+ - Ca^{2+}$ exchanger, taking calcium in and Na^+ out. Through this mechanism, hypoxia increases intracellular calcium concentration. In the model, we present these mechanisms as a single reaction considering an inversely proportional relationship between oxygen levels and calcium increase in the cytoplasm.

3.7. Note on nomenclature

In this work, we consider a model of two endothelial cells, with the goal of representing their interaction during angiogenesis. Initially, we stimulate one of the cells with a higher amount of VEGFA than the other to evaluate the different signals guiding their interaction. The cell that receives a higher initial stimulus is referred to in this study as the stimulated cell, first cell, or tip cell. The cell initially receiving less VEGFA is referred to as the unstimulated cell, second cell, or stalk cell.

4. RESULTS

4.1. Model construction

The model was designed based on previous mechanistic models (Bazzazi et al., 2017, 2018; Zhao and Popel, 2015; Venkatraman et al., 2016) of EC signaling. Figure 2 shows the pathways included in the model.

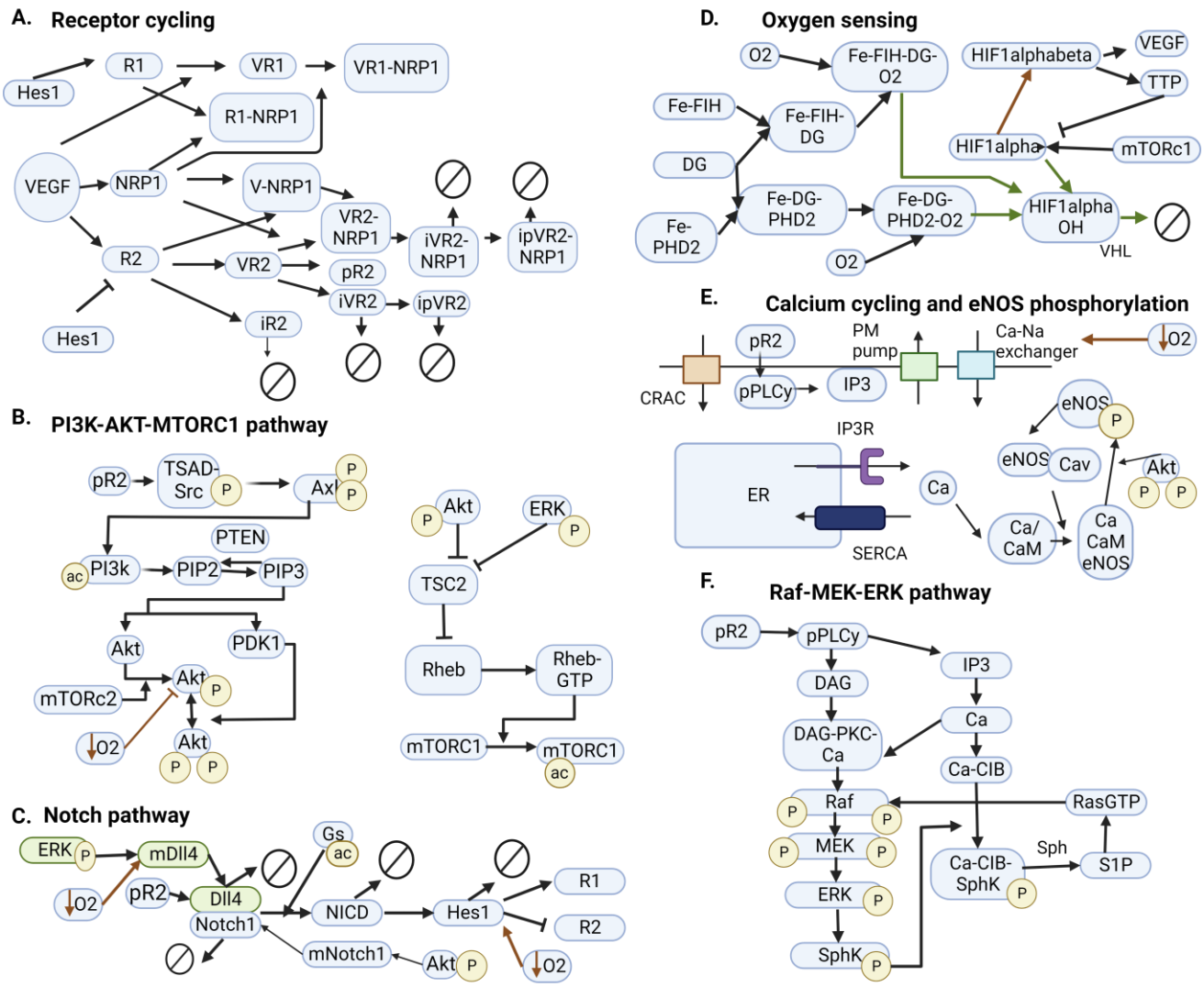

Figure 2. Pathways included in the model. (A) VEGF interacting with VEGFR1, VEGFR2, and NRP1. Inhibition of VEGFR2 by Hes1 and upregulation of VEGFR1. (B) Pathway leading to the downstream phosphorylation of Akt on ser473 and thr308 and activation of mTORC1. (C) Notch signaling pathway influenced by hypoxia. Green and blue colors represent different cells. (D) HIF signaling pathway leads to the production of VEGFA. Solid green lines indicatenormoxia-induced events. Red dashed lines indicate hypoxia-induced events. (E) Calcium cycling module including current through the CRAC channels and PM pump, endoplasmic reticulum calcium cycling through SERCA and IP3R, and indirect stimulus of IP3 by VEGF. Na^{+}-Ca^{2+} exchanger increases intracellular calcium concentration under hypoxia. (F) MAPK-ERK signaling pathway interacting with the calcium cycling module.

Overall, the model describes the regulation and coordination by Notch and HIF1-α of the cell interactions and downstream signaling. The model comprises two representative cells, initially configured similarly and later stimulated by different concentrations of VEGF, and is divided into 6 modules: the Notch pathway, the oxygen sensing module, the VEGF-VEGFR pathway, the Akt-eNOS pathway, the Raf-MEK-ERK, and the calcium cycling module. The oxygen

327 sensing module integrates the previously established model by Zhao and Popel (Zhao and Popel,
328 2015), adding a mammalian target of rapamycin complex 1 (mTORC1).

329 The VEGF-VEGFR module includes VEGF signaling by surrounding cells (e.g.,
330 macrophages), binding to VEGFR2, VEGFR1, and neuropilin (NRP1) on the cell's surface. Once the
331 VEGF-VEGFR2 complex is formed, that leads to the phosphorylation of VEGFR2, affecting all other
332 modules. The phosphorylated receptor will lead to the subsequent phosphorylation of Src, Axl,
333 PI3K, PIP2 and Akt. It will also activate the MAPK-ERK signaling, causing the phosphorylation of
334 PLCγ, Raf, MEK, Erk, and sphingosine kinase (SphK) and activation of IP3. IP3 activation regulates
335 the calcium cycling module, shown in Figure 2D. The calcium cycling module shows the circulation
336 of calcium between the cytoplasm and endoplasmic reticulum of the cell. This module was
337 designed according to the version presented by Bazzazi et al. (Bazzazi et al., 2017).

338 The phosphorylation of Akt and Erk leads to the activation of mTORC1, which will then
339 upregulate HIF-1α in the cytoplasm. In our model, we assume that this is the main production
340 source of HIF-1α. Finally, the phosphorylated Erk will cause an upregulation of Dll4 expressed on
341 the cell surface, and phosphorylated VEGFR2 upregulates filopodia formation. The expressed Dll4
342 will bind to Notch receptors on the surface of the second cell. The enzyme $\gamma_{secretase}$ cleaves the
343 intracellular domain of the Notch receptor, which translocates to the nucleus and leads to the
344 expression of Hes1. Hes1 inhibits the expression of VEGFR2 in the adjacent cell surface,
345 diminishing its interaction with VEGF. Notch signaling is also known to increase the expression of
346 VEGFR1 in the stalk cell, which is also represented in the model (Blanco and Gerhardt, 2013). This
347 process contributes to a controlled interaction with VEGF, and the organized formation of
348 sprouts. This interaction will determine the EC fate, with one of the interacting cells assuming
349 the tip position (the cell with a greater amount of Dll4 and filopodia) and the other a stalk position
350 (in which Notch signaling is upregulated leading to less VEGFR2 and NRP1 available for
351 phosphorylation, and more VEGFR1). As discussed, the model integrates 6 major pathways that
352 interact with each other, promoting cell differentiation and signaling. In this work, we will initially
353 focus on the model behaviors under the influence of Notch signaling and VEGF signaling under
354 normoxia, followed by an analysis of cell signaling under hypoxia.

355 ## 4.2. Model parameterization and sensitivity analysis
356

357 We performed structural identifiability analysis on 60 unknown parameters in our model, using
358 4 Lie derivatives and 44 observables. We used GenSSI2 to perform structural identifiability
359 analysis, a toolbox based on the generating series approach coupled with the use of identifiability
360 tableaus, as described by its developers (Balsa-Canto et al., 2010)(Balsa-Canto et al., 2010)(Balsa-
361 Canto et al., 2010)(Balsa-Canto et al., 2010)(Balsa-Canto et al., 2010)(Balsa-Canto et al.,
362 2010)(Balsa-Canto et al., 2010)(Balsa-Canto et al., 2010)(Balsa-Canto et al., 2010) (Balsa-Canto et
363 al., 2010) (Balsa-Canto et al., 2010) . Our analysis identified 11 globally identifiable parameters
364 (marked in Supplementary material parameters). Subsequently, we fit the model parameters
365 that are identifiable and estimate the remaining parameters based on literature data, as

366 referenced in the supplementary material. Figure S3 shows the identifiability tableau generated
367 by GenSSI2. We estimated the values of parameters indicated as non-identifiable by GenSSI2 to
368 improve fitting results based on literature data. Parameters with values not available in the
369 literature were estimated to optimize the fitted response-curve related to them.

370 To determine model parameters, we fit the model to experimental data from human endothelial
371 cells (HUVECs) and retinal endothelial cells available in the literature (see Figures 3,4). All data
372 simulated were normalized to their maximum concentration for comparison with literature data.
373 We obtained the initial absolute concentrations in units of µM from previous mechanistic models
374 of endothelial cells and data from the literature. Initial VEGF receptor values were estimated as
375 6000 VEGFR2/cell and 2000 VEGFR1/cell (Imoukhuede and Popel, 2011), considering a cell area
376 of 1000µm2, with $1 * 10^{-12}$L volume. Neuropilin-1 density per cell has been estimated in the range
377 of $10^3 - 10^6$ number per cell (Gabhann & Popel, 2006). Starting at an initial estimate of 25000
378 receptors per cell (Imoukhuede & Popel, 2011), we fit the initial concentration of Neuropilin1,
379 for both cells, obtaining 0.0664 µM as the initial molar concentration, equivalent to about 40000
380 receptors per cell in both cells. Quantifying an absolute number of surface receptors in specific
381 cell types can be challenging, despite recent efforts (Chen & Imoukhuede, 2019). We evaluate
382 this aspect by inspecting the sensitivity of Hes1 in both cells to changes in VEGFR2 concentration,
383 as an additional analysis (Figure S4).

384 To show cell differentiation based on higher VEGF sensing, all species concentrations are
385 considered initially the same for the two interacting cells. To simulate cell patterning, we consider
386 an initial stimulus of 0.0012µM of VEGF for the first cell, while the second cell is set to a 0.0006µM
387 stimulus. This different stimulation allows us to analyze the Notch signaling pathway effects on
388 EC patterning. As we could not find absolute concentrations for Notch1 receptors on the surface
389 of EC during angiogenesis, we estimated the initial concentration to be about the same as that
390 of VEGFR2 receptors (0.0099µM). mRNA Dll4 and protein Dll4 initial values were initially zero for
391 both cells.

392 The model is fitted under normoxia (21% O_2), with VEGF stimulation (50ng/ml), and
393 hypoxia (1% O_2), also with VEGF stimulation. The data used for calibration accounts for more than
394 200 data points from 19 different studies presenting time-course data. Given the amount of
395 stimulation by VEGF given to each cell, we perform and present the fitting to the species in the
396 first cell, stimulated with VEGFA 50ng/ml.

397

398

399 4.2.1. VEGF-driven pathway under normoxia

400 Using global Particle Swarm Optimization, we initially fit the model under normoxia conditions
401 ($[O_2]$ = 209µM) for stimulation with 50ng/ml of VEGFA. Figure 3 presents the time dynamics of

the fitted species compared to the experimental data. By each time-course panel, we present the Runs test results to show the goodness of fit.

The time dynamics of Notch-related pathways are shown in panels Figure 3A,B,D,N. Endothelial cells stimulated by VEGFA present an increase in the activation of the Notch signaling pathway, increasing NICD and Hes1 expression, which peak during the first hour of stimulation, and then decay (Takeshita et al., 2007; Izumi et al., 2012). Additionally, VEGFA stimulation is known to increase the expression of Dll4 mRNA through the ERK pathway (Fish et al., 2017).

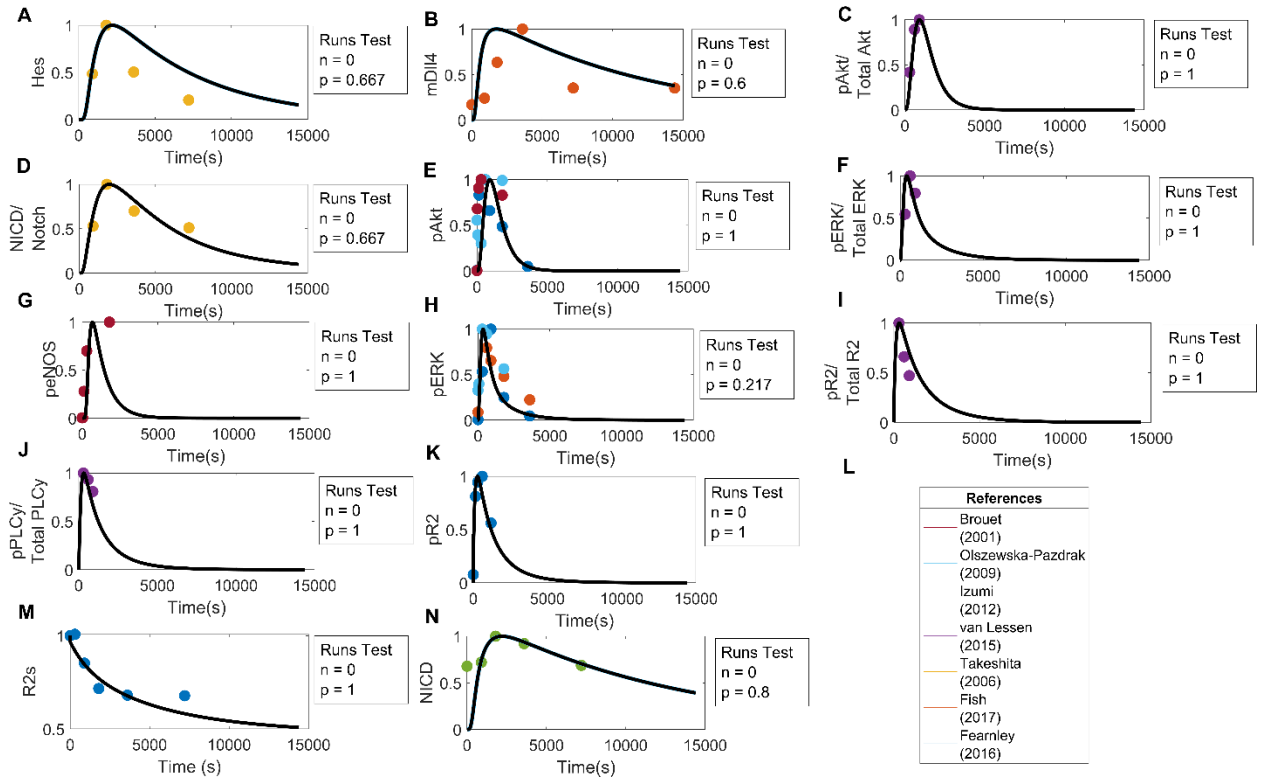

Figure 3. Model time-course simulation post-fitting and literature experimental data on VEGFA-induced (A) Hes1 upregulation Takeshita et al. (2007); (B) mDll4 upregulation Brouet et al. (2001); (C,E) upregulation of phosphorylated Akt Van Lessen et al. (2015) ; Brouet et al. (2001) ; Fearnley et al. (2016) ; Olszewska-Pazdrak et al. (2009); (D,N) upregulation of relative NICD Takeshita et al. (2007); Izumi et al. (2012). (F,H) upregulation of phosphorylated ERK1/2 Van Lessen et al. (2015); Olszewska-Pazdrak et al. (2009); Fish et al. (2017); Fearnley et al. (2016); (G) eNOS increase in phosphorylation Bartoszewska and Kochan (2014); (I,K) VEGFR2 increase in phosphorylation Van Lessen et al. (2015); Fearnley et al. (2016); (J) increase in relative PLCγ phosphorylation; and (M) decrease in free surface VEGFR2.

Other events stimulated by VEGFA include the phosphorylation of VEGFR2 (panel I), Akt (panels C and E), and ERK1/2 (panels F and H) (Van Lessen et al., 2015; Olszewska-Pazdrak et al., 2009; Fearnley et al., 2016). Given VEGFR2 phosphorylation, the calcium signaling pathway is activated and influences eNOS phosphorylation (panel G) (Brouet et al., 2001). The rapid phosphorylation of VEGFR2 causes the decrease of the free surface receptors, shown in panel M (Fearnley et al., 2016).

4.2.2. Hypoxia-driven pathway

Under hypoxia ([O_2] = 9.9uM), several events occur in endothelial cells, as previously discussed. Given our interest in better understanding EC patterning under hypoxia, we calibrate the model parameters to data from endothelial cells under hypoxia. The results are presented in Figure 4.

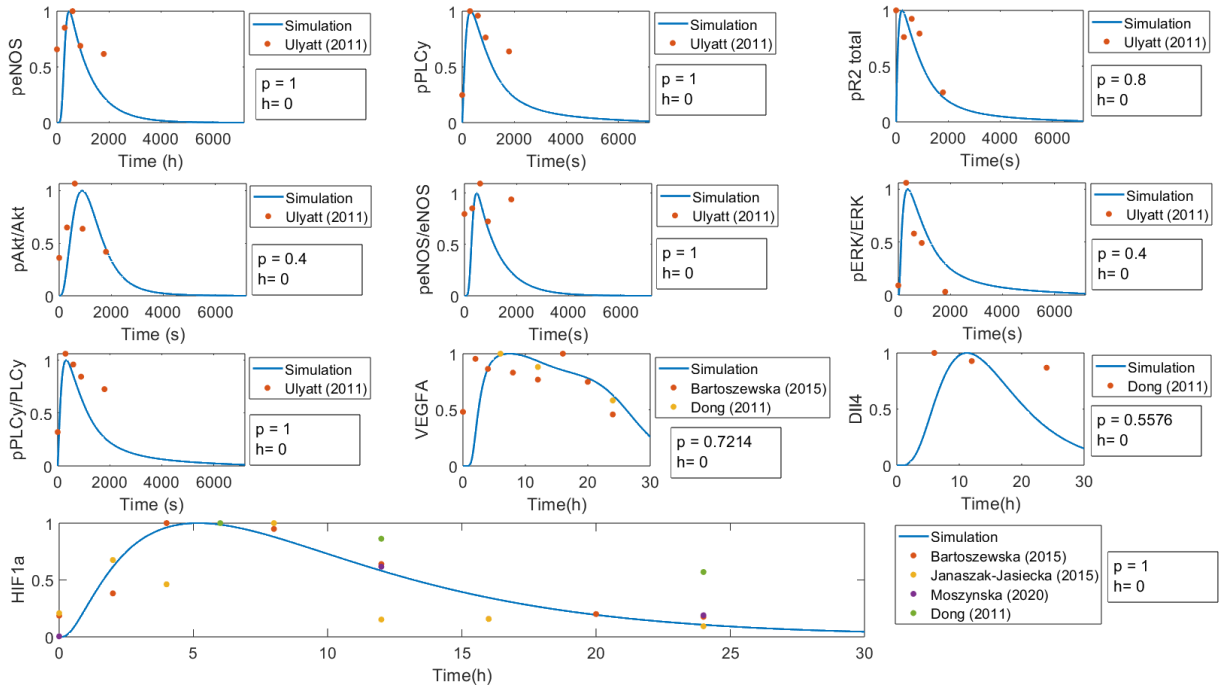

Figure 4. Fitting model to experimental data under hypoxia. Model time-course simulation post-fitting and literature experimental data on hypoxia-induced (A) phosphorylated eNOS, (B) phosphorylated PLCγ, (C) phosphorylated VEGFR2, (D) VEGFA produced by the endothelial cell, (E) relative phosphorylated Akt to total Akt, (F) relative phosphorylated eNOS to total eNOS, (G) HIF1α, (H) relative phosphorylated ERK1/2 to total ERK1/2 and (I) relative phosphorylated PLCγ to total PLCγ.

Endothelial cells under hypoxia sense the low oxygen levels through the HIF1α signaling pathway, which will lead to an increase in the concentration of HIF1α (panel G) and downstream release of VEGFA (panel D). Cells stimulated with VEGFA under hypoxia also present an increase in the phosphorylation of VEGFR2 (panel C), phosphorylation of eNOS (panels A and F), and phosphorylation of PLCγ (panels B and I). Coherently, the concentration of phosphorylated Akt and ERK1/2 also increases (panels E and H). Limited data is available for the time course of proteins from the Notch signaling pathway under hypoxia. However, experiments by Patel and colleagues showed an increase in Dll4 under hypoxia (Patel et al., 2005).

4.2.3. Global sensitivity analysis of ECPI

445 We performed a global sensitivity analysis with PRCC on the ECPI of both interacting cells under
446 hypoxia conditions to evaluate which reactions had a higher effect on determining cell
447 patterning. The ECPI represents each cell's tip/stalk markers ratio based on the concentration of
448 Dll4, VEGFR2, and Hes1. We present the PRCC values of parameters with a p-value smaller than
449 0.05 in Figure 5. Figure 5A presents the parameters with higher or lower PRCC values in at least
450 one of the cells. For comparison, we group the bar plots showing the ECPI of both cells at 1 hour
451 and 2 hours under hypoxia, depending on the parameter. The time points were selected to
452 indicate a moment where Hes1 is evidently distinct between the two cells (1 h) and one moment
453 when Hes1 values are similar between the two cells, indicating competition for the tip position
454 (2 h). Therefore, the parameter might be more influential ($p<0.05$) for one cell but not the other
455 (as can be seen for the degradation rate of $\gamma_{\text{secretase}}$- kdeg_Gs). The pathways related to the
456 parameters described in each panel are color-labeled for clarity. Figures 5b and 5c present our
457 PRCC results for the reaction equivalent to the parameter identified as the most influential for
458 either of the cells. The top 10 positive or negative PRCCs are shown for each cell, evaluated at 1
459 hour or 2 hours under hypoxia, totalizing 20 reactions per cell per time point.

460 Based on the results presented in Figure 5a, the most influential parameter on ECPI
461 determination, regardless of time or cell, is the Hill coefficient n in the reaction of VEGFR2
462 inhibition by Hes1 expression. Binding and unbinding rates of VEGFR2 to NRP1 and receptor (in
463 complex with NRP1) internalization rate are also relevant. Interestingly, the formation rate of
464 $\gamma_{\text{secretase}}$ and the degradation rate of internalized phosphorylated VEGFR2 present an opposing
465 effect on the ECPI of the two cells under 1 h of hypoxia, which is not seen later, at 2 h, an
466 indicative of the time-dependence (either due to hypoxia or to competition between the two
467 cells).

468 While some of the most significant reactions are common for both the stimulated and
469 unstimulated cell (VEGFR2 inhibition by Hes1, binding and unbinding of Neuropilin1-VEGFA to
470 VEGFR2 and internalization of complex VEGF-NRP1-VEGFR2), some differ. Regarding the
471 pathways that most show up for each cell when assessing the top 10 PRCCs (Figures 5b and 5c),
472 the results indicate that the ECPI for both cells at 1 or 2 hours under hypoxia is mostly affected
473 by reactions in the VEGFR2 pathway. Regarding PRCC values, the inhibition of VEGFR2 by Hes1 (a
474 reaction in the Notch pathway) is the most significant overall for determining both cells' ECPI.
475 Reactions in the HIF1α pathway appear significant for both cells in both time points evaluated,
476 reiterating the importance of oxygen levels on cell patterning. Reactions that directly affect the
477 concentration of VEGFR2 (e.g., degradation of VEGFR2, binding/unbinding to VEGF and NRP1,
478 and receptor internalization) are, however, the most influential for pattern definition in the cells,
479 which is in agreement with previous studies on endothelial cell patterning.

480

481

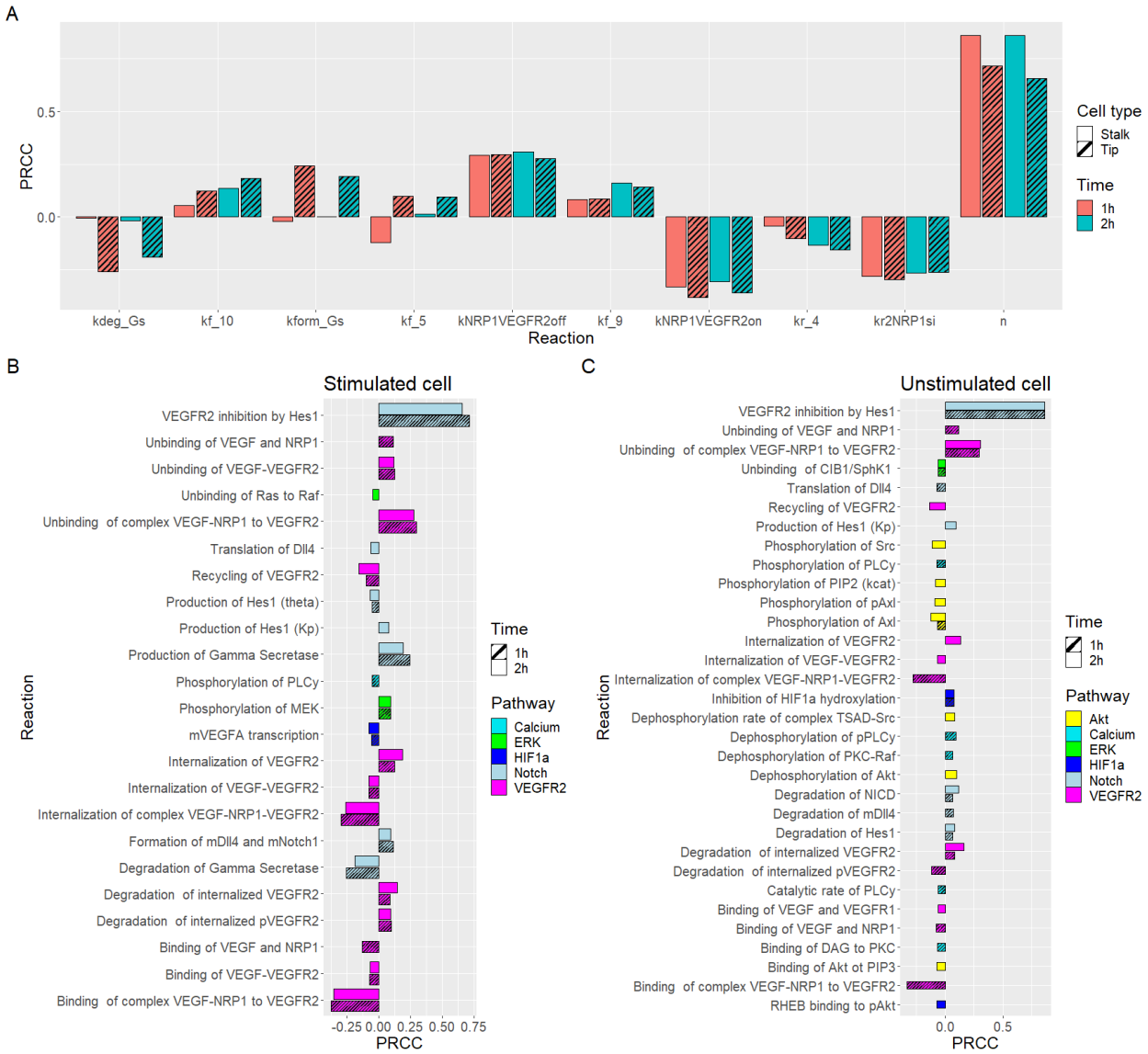

Figure 5. Sensitivity indices ($p < 0.05$) of parameters controlling the ECPI under hypoxic conditions for the stimulated and the unstimulated cell at different time points. The colors indicate respective pathways related to the parameters, and cell type is indicated by a dashed (stimulated cell) or non-dashed (unstimulated cell) pattern. (A) PRCC values for the top 10 most relevant parameters which influence pattern in at least one of the cells, compared to the same parameter on the other cell at 1h and 2h under hypoxia. Twenty most influential reactions (top 10 + and top 10 -) that influence ECPI of the stimulated cell (B) or the unstimulated cell (C) at 1h or 2h under hypoxia. kdeg_Gs: degradation rate of $\gamma_{\text{secretase}}$. Kf_10: Internalization rate of VEGFR2. Kform_Gs: production rate of $\gamma_{\text{secretase}}$. kf_5: Degradation rate of internalized phosphorylated VEGFR2. kNRP1VEGFR2on/off: Binding/unbinding rate of complex VEGF-NRP1 to VEGFR2. kr_4: Recycling rate of internalized VEGFR2. kf_9: Degradation rate of internalized VEGFR2. kr2NRP1si: Internalization rate of complex VEGF-NRP1-VEGFR2. n: Hill coefficient for Hes1 inhibition of VEGFR2.

The common, most significant reaction that influences the ECPI is the inhibition of VEGFR2 by Hes1. This is consistent with the established context of endothelial cell patterning (Wang et

al., 2022), regardless of hypoxia. The inhibition of VEGFR2 by Hes1 affects all pathways downstream of VEGFR2 phosphorylation and VEGFR1 and NRP1 binding to available VEGFA. Notch signaling itself is affected by it, as Dll4 expression depends on ERK1/2 phosphorylation (which is downstream of VEGFR2 phosphorylation). That is also revealed by the ERK pathway-related reactions at the tip cell (phosphorylation of MEK) and stalk cell (unbinding of CIB1-SphK1, upstream of ERK phosphorylation). Other than reactions in the VEGFR2 signaling pathways, several reactions from the calcium signaling pathway affect the ECPI of the unstimulated cell but are not as present in the top reactions related to the ECPI of the stimulated cell (comparing Figures 5b and 5c). The sensitivity analysis shows that at 1 hour under hypoxia, VEGFR2 inhibition by Hes1 is slightly more influential on the ECPI of the stimulated cell than at 2 hours, while it is similarly influential at both times for the unstimulated cell. Additionally, our results indicate that time under hypoxia affects the reaction influence on pattern definition. For instance, binding/unbinding of VEGF and NRP1, unbinding of Ras to Raf, translation of Dll4, phosphorylation of PLCγ and Hes1 production only appear at one of the two time points on the top 10 PRCCs of the stimulated cell (Figure 5b). For the unstimulated cell, most reactions tend to appear relevant at only one of the time points (Figure 5c). The results support that time influences cell patterning as they compete for the tip position.

Our PRCC analysis also indicates a difference in the top Notch-related reactions' sensitivity between the two cells regarding $\gamma_{\text{secretase}}$ production and degradation. While the first cell presents a higher absolute PRCC for $\gamma_{\text{secretase}}$ reactions, the second cell presents PRCC values for the same reaction-related parameters less than 0.01 (Supplementary Material PRCC and p-values). Additionally, our results indicate that the unstimulated cell's ECPI is influenced by several Akt-related reactions (Figure 5c), which are not seen for the stimulated cell top 10 (Figure 5b).

4.3. Cell patterning: tip and stalk endothelial cells

Sprouting angiogenesis requires a well-orchestrated balance of tip and stalk EC. Recently, Xu and Li (2022) employed network-based analysis to assess the genetic signature in the tip and stalk EC, contributing to their different signaling. While tip cells presented up-regulated genes related to pathways such as MTORC1 and PI3K-Akt-MTOR signaling, stalk cells showed up-regulated genes in the Notch signaling pathway and angiogenesis (among others). Notch signal upregulation in stalk cells agrees with the previous work of del Toro et al. (2010), which performed transcriptome analysis on murine ECs. The lack of Dll4 contributes to the formation of tip EC, limiting Notch signaling. Additionally, tip/stalk patterning is regulated by several other mechanisms, which directly or indirectly interact with the Notch signaling pathway. For instance, VEGF-VEGFR2 downstream pathways (PI3K-Akt and ERK) regulate not only the proliferation and migration of EC, but also the expression of tip cell genes such as Dll4 (Margadant, 2020). Calcium oscillations

also play a role in EC patterning and vessel architecture (Debir et al., 2021), and loss of eNOS has been shown to suppress tip EC polarization in bovine ECs (Smith et al., 2022; Priya et al., 2015).

Our model aimed to show, initially, such patterning behavior of the two interacting endothelial cells represented. For that, we set both cells to similar initial conditions (species and parameters). We then stimulated one cell with a higher VEGF concentration (one order of magnitude higher), as previously described, and register the distinct signaling of both cells. Figure 6 shows the time courses for phosphorylated VEGFR2, Dll4, NICD and Hes1 for both cells under normoxia and hypoxia.

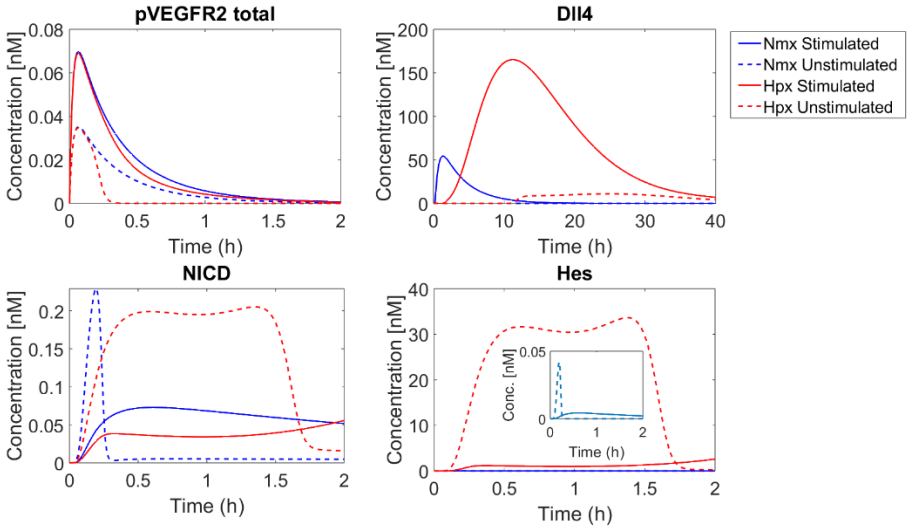

Figure 6. Endothelial cell patterning under normoxia and hypoxia. Concentration time dynamics in tip and stalk cell of (A) phosphorylated VEGFR2 (pR2), (B) Dll4, (C) Notch intracellular domain (NICD), and (D) Hes1. The inset zooms in on the dynamic concentration of Hes1 under normoxia. Blue lines represent normoxia, and red lines represent hypoxia. Solid lines refer to the stimulated cell, while dashed lines refer to the unstimulated cell.

The two cells present different concentration dynamics over time of the analyzed proteins. The stimulated cell presents, in both normoxia and hypoxia, increased levels of phosphorylated VEGFR2 and Dll4, while the unstimulated cell presents higher NICD and Hes1 levels, consistent with the expected behavior of tip and stalk endothelial cells (Akil et al., 2021; Venkatraman et al., 2016).

Our simulations also show that hypoxia prolongs the expression of Dll4 in both cells, changing the peak time (panel B). Accordingly, NICD and Hes1 under hypoxia show prolonged-expression when compared to normoxia. An increase in the concentration of each parameter evaluated is also evident for both cells. Hypoxia accelerates the phosphorylation of VEGFR2, shown by its fast decay (more evident in the unstimulated cell) compared to the normoxia curve

(panel A). This behavior is likely due to increased Hes1 expression in the unstimulated cell during hypoxia (panel D), matching the expected stalk cell behavior.

As the initial amount of VEGFA provided to both cells decreases and reaches lower values for the initially stimulated cell (first cell) than for the initially unstimulated cell (second cell), we note a behavior change, with the amount of Dll4 becoming higher in the second cell, while NICD and Hes1 become higher in the first cell. This represents cell-cell competition for the tip position, which has been reviewed by Blanco and Gerhardt (2013) and modeled by Jakobsson et al. (2010).

4.4. Hypoxia-induced signaling

The effect of hypoxia on the Notch signaling pathway and how it affects other pathways is investigated in this section. For the simulations in this section, 50ng/ml of VEGF was added to the first cell, with both cells starting at low oxygen concentration (1% O_2, equivalent to 9.9µM) for 48 h. Figure 7 shows the simulation of protein concentration dynamics under hypoxia conditions for both tip and stalk EC.

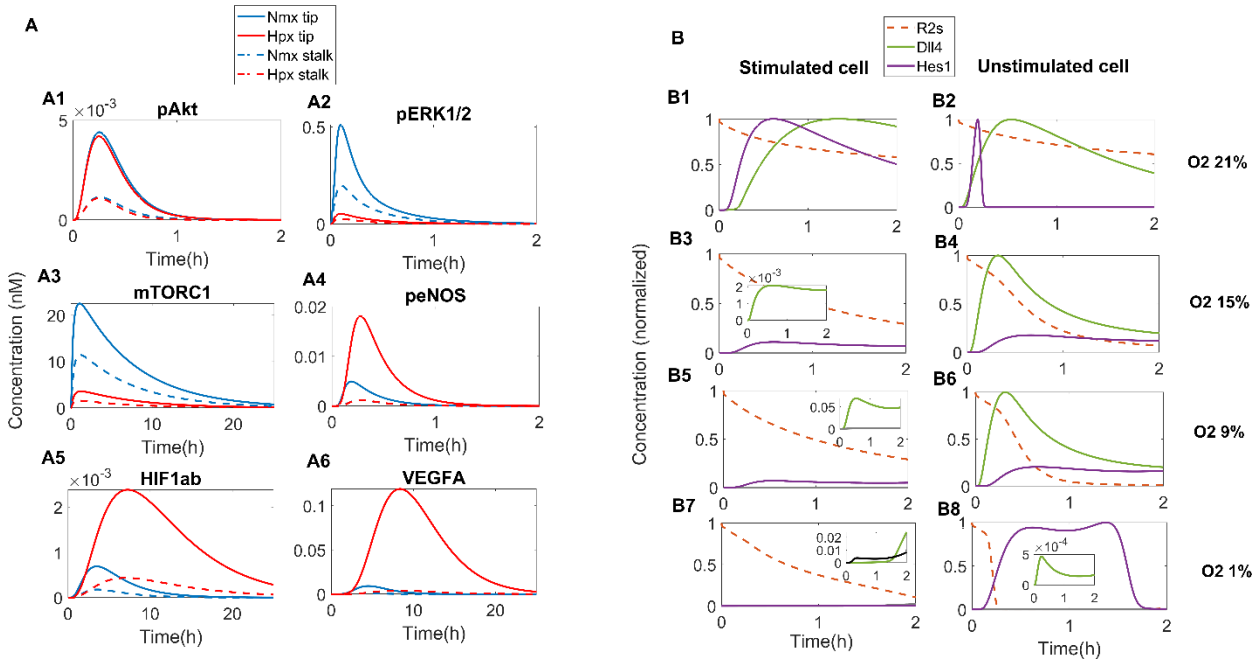

Figure 7. Hypoxia alters the signaling behavior of cells. (A) Dynamics of pAkt (panel A1), pERK1/2 (panel A2), mTORC1 (panel A3), peNOS (panel A4), HIF1ab (panel A5), and VEGFA (panel A6) in both cells under normoxia (blue) and hypoxia (1% O_2) (red). Solid lines refer to the stimulated cell, and dashed lines to the unstimulated cell. (B) Normalized concentration of surface VEGFR2, Dll,4 and Hes1 in tip (left) or stalk (right) virtual cells, under normoxia (panels B1 and B2), 15% O_2 (panels B3 and B4), 9% O_2 (panels B5 and B6) or 1% O_2 (panels B7 and B8). Insets are presented in the same time units as panels, and concentration is relative to their maximal concentration during the simulated periods.

583 For both cells, hypoxia leads to a slight decrease in total phosphorylated Akt (panel A1),
584 and a larger decrease in mTORC1 and ERK1/2 phosphorylation (panels A2 and A3). The
585 phosphorylation of eNOS increases considerably, with higher phosphorylation on the tip cell,
586 compared to the stalk cell (panel A4). The reduced oxygen causes an increase in the formation of
587 complex HIF1αβ in the nucleus, as shown in panel A5. Consequently, there is an increased
588 production of VEGFA by the cell (panel A6). The simulations in panel A consistently show higher
589 levels of proteins for the tip cell, when compared to the stalk cell, regardless of the oxygen
590 concentration level.

591 Now we investigate the relative changes in surface VEGFR2, Dll4, and Hes1 in both cells
592 kept at different oxygen concentrations for 2 h (panel B). To evaluate the behavior comparatively,
593 the curves are normalized to their maximum concentration during the simulated period (48 h).
594 Panels B1, B3, B5, and B7 present the simulated results for the first cell (receiving higher
595 stimulation) and panels B2, B4, B6, and B8 the results for the second cell. The oxygen
596 concentrations for each simulation are shown on the right.

597 The simulations show that for both cells, as the level of hypoxia-induced increases, the
598 concentration of free surface VEGFR2 decreases more rapidly. Dll4 has a dynamic behavior
599 depending on the oxygen level. The decay is faster in the unstimulated cell than for the
600 stimulated cell, as the hypoxia level decreases. For the stimulated cell, at 21% O_2, Dll4 peaks
601 between one and two hours. At lower oxygen levels, the Dll4 peaks at later time points (after 2h),
602 and during the 2 h simulated, it reaches 0.2% (panel B3), 5% (panel B5), and 2% (panel B7) of the
603 peak value. For the second cell, such prolonged time to reach a peak value is not seen for 15% O_2
604 (panel B4) and 9% O_2 (panel B6), only for 1% O_2, in which case it reaches a maximum of 0.05% of
605 its peak value during the initial 2 h of simulation (panel B8).

606 Hes1 reaches its peak value during the first two hours of simulation under normoxia in
607 both cells, and for 1% O_2 the unstimulated cell Hes1 values also reach a peak during the initial 2
608 h. For other oxygen concentrations, both cells take over 2 h to reach their peak Hes1 values.
609 Comparatively, the relative amount of Hes1 concentration to its maximum (at 15% and 9% O_2) of
610 the stimulated cell is lower during the initial 2 h than that of the unstimulated cell. Under
611 normoxia, Hes1 presents a more prolonged duration for the stimulated cell than for the
612 unstimulated cell.

613 4.5. Oxygen levels, time and stimulation changes the protein signaling and ECPI of the
614 interacting cells
615

616 We then evaluate the effects of hypoxia on the ECPI of both cells. The ECPI is calculated at
617 different time points for each cell, at different oxygen concentrations, and normalized to a
618 baseline. The baseline is defined as the maximum ECPI value between the two cells at each
619 condition. After normalizing to the baseline, for visualization purposes, we calculate the
620 exponential of the normalized result. This final result is plotted in the bar plots at Figure 8A.

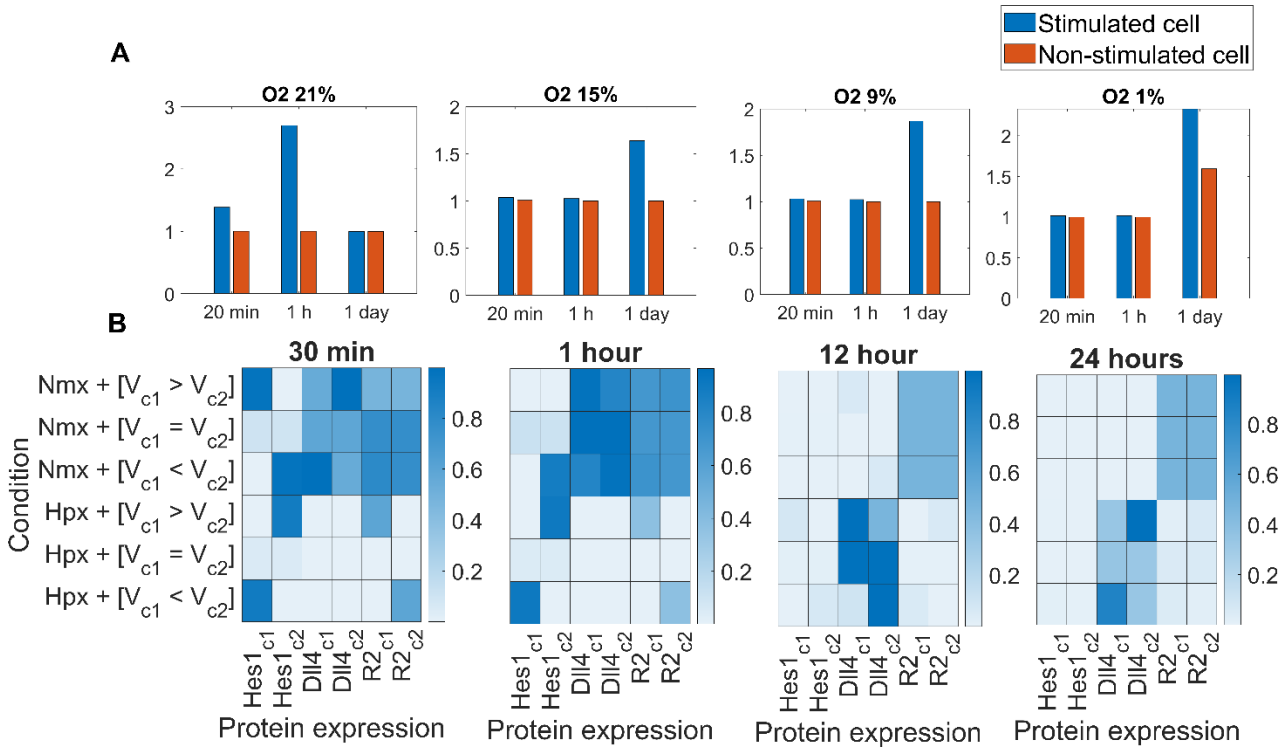

Figure 8. Time, stimulation, and hypoxia play a role in cell patterning and protein expression. (A) ECPI changes in tip and stalk cells at different oxygen concentrations and stimulation times. (B) Change in proteins expression pattern for 24 h given 6 different conditions. + sign indicates concomitant stimulation. Nmx = normoxia; Hpx = hypoxia; c1 = first cell; c2 = second cell; Vx > Vx represents that the first cell receives higher VEGFA stimulation than the second cell and vice-versa.

The simulated results show a change on the ECPI of the cells as time passes, and at different oxygen concentrations. Under normoxia, the stimulated cell presents a higher ECPI than the unstimulated cell, with a higher difference seen at 1 h of simulation. At 1 day of simulation, the normalized ECPIs of both cells become about the same as the basal level. At hypoxia levels, the initial difference between the two cells seen at normoxia is reduced during the initial 20 min and 1 h of simulation, and the difference increases at 1 day of simulation. At 1% O_2, the relative ECPI increases for both cells for 1 day of simulation.

To explore the changes in ECPI under normoxia and hypoxia for the two cells, we simulate 6 different scenarios (3 under normoxia and 3 under hypoxia), varying which cell received the higher amount of VEGFA stimulation and how that affected the expression of Hes1, Dll4, and VEGFR2 at each cell. The values are normalized to their maximum value during a 48 h simulation.

Figure 8 presents the simulations for 30 min, 1 h, 12 h and 24 h. The cell response under these six conditions shows that hypoxia, VEGFA stimulation and time itself define the cell patterning through changes in protein expression. This also indicates that the ECPI sensitivity of interacting cells depends on these factors and might change considerably at different times and oxygen levels.

643 4.6. Inhibition of Notch signaling by DAPT under normoxia and hypoxia conditions
644

645 A small molecule DAPT works as a competitive inhibitor that binds to $\gamma_{secretase}$, impeding the
646 cleavage of NICD (Paresi, 2016). Through its action, it is possible to induce tip cell patterning
647 (which is usually inhibited by the Notch downstream signaling). For assessing the action of DAPT
648 on stimulated and unstimulated cells, we simulate the NICD/Notch (amount of intracellular
649 domain relative to total Notch1 receptor) response of both cells to different amounts of DAPT.
650 The time course is shown in Figure 9A,B. Panel C compares experimental data from Takeshita et
651 al. (2007) of relative NICD to total Notch1 at different concentrations of DAPT to simulated
652 results.

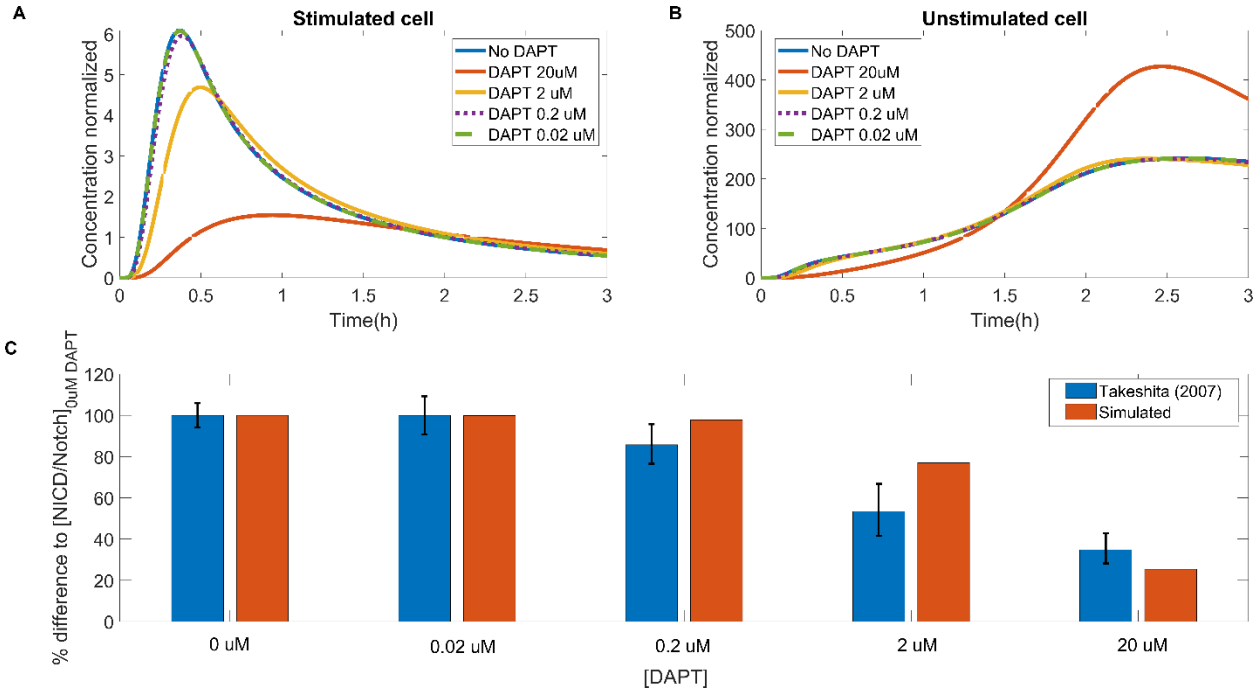

653

654 Figure 9. The effect of DAPT on inhibiting Notch cleavage by $\gamma_{secretase}$. Using the same concentration of
655 DAPT in the two interacting cells, we simulated their responses (NICD relative to total Notch1) over 3 h.
656 (A) NICD/Notch1 measured in the VEGFA-stimulated cell, compared to (B) NICD/Notch1 measured in the
657 less stimulated cell. (C) Model calibration against experimental data of NICD relative to total Notch1 given
658 DAPT cleavage inhibition.

659 Panel A shows the response of the first cell in the system (receiving a higher VEGFA
660 stimulation - 50 ng/ml). The response is proportional to the dosage of DAPT used for inhibition
661 of the cleaving enzyme: as the concentration of inhibitor increases, the cleaving enzyme activity
662 decreases and less Notch intracellular domain is cleaved from the receptor. The peak
663 concentration of NICD relative to Notch1 is seen during the first hour of simulation.
664 Comparatively, the second cell presents a contrasting behavior, with peak values of NICD/Notch1
665 after 2 h of stimulation with DAPT. Additionally, the peak relative concentration of NICD is
666 recorded for DAPT 20µM, the highest amount of inhibitor. This behavior suggests that treating

both cells with DAPT concomitantly for 3 h affects their interaction, increasing the amount of relative NICD on the second cell for a certain period if compared to smaller DAPT dosages.

4.7. Interventions to induce specific cell patterns

Controlling endothelial cell patterning is a potential strategy for controlling sprouting angiogenesis and capillary stability. Several strategies have been used for promoting angiogenesis in the past years, and those directly affecting the Notch signaling pathway are of interest to the present study. Since hypoxia and VEGF stimulation affect interacting-cells patterning, we simulated 3 interventions that could affect the signaling and pattern definition. As we wish to observe differences in response between normoxia and hypoxia, as well as the time under each condition, we simulate each of three interventions at normoxia and hypoxia for 1 h, 12 h, and 24 h simulations. The model is also calibrated to experimental data on inhibition of ERK phosphorylation (using 40nM of siERK1/2) (Fish et al., 2017) and $\gamma_{\text{secretase}}$ inhibition using DAPT (20uM) (Takeshita et al., 2007). The fitted response of Dll4 and NICD/Notch1 are shown in Figures 9C and 10A, respectively.

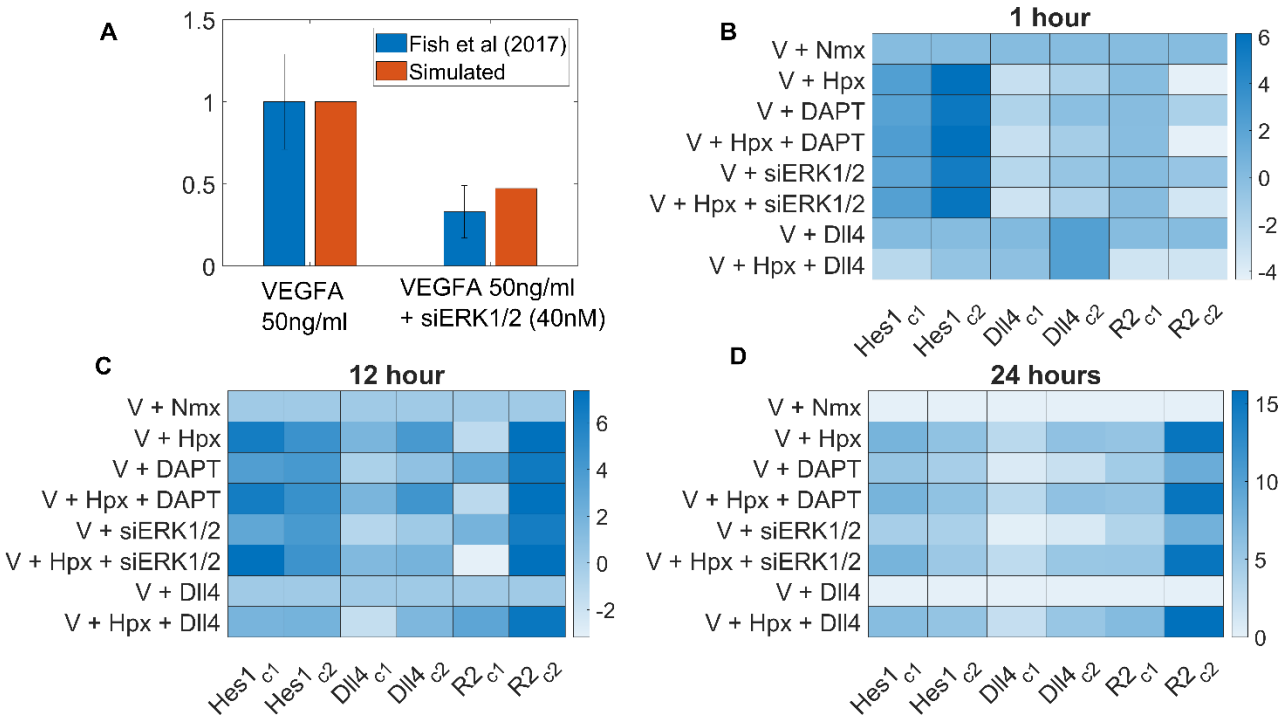

Figure 10. Response of stimulated and unstimulated cells to DAPT, siERK, and Dll4 under hypoxia and normoxia. (A) Dll4 response to siERK1/2 combined with VEGFA stimulation for 1 h. VEGFA stimulated model response of Hes1, Dll4 and VEGFR2 on both cells to DAPT (20 µM), siERK1/2 (40 nM) and Dll4 (0.2 µM) under normoxia and hypoxia for (B) 1 h, (C) 12 h or (D) 24 h. The concentrations were normalized to normoxia values at the equivalent simulated time point and log10 normalized.

Our results show that, for all three periods evaluated, hypoxia is able to up-regulate Hes1 in both cells when compared to normoxia values. This agrees with previous findings on the relation between Notch signaling and hypoxia, with the increase in Hes1 levels being context-dependent (O'Brien et al., 2022; Jögi et al., 2002; Gustafsson et al., 2005). Our model also indicates time dependence of the response to hypoxia. For instance, during the first hour of simulation, hypoxia down-regulated Dll4 and VEGFR2 in both cells (negative values on Panel B), but an increase is noted at 12 h and 24 h (except for VEGFR2 in the first cell at 12 h, shown in panel C). The increase in Dll4 under hypoxia has been reported in the literature (Patel et al., 2005) for different cell types, but not the time-dependency here noted. Considering that higher values of Dll4 and VEGFR2 available are linked to the tip cell pattern, while the higher expression of Hes1 is related to the stalk cell pattern, we observe that at 1 h of stimulation, hypoxia, DAPT, and siERK1/2 stimulation conditions indicate a higher Hes1 concentration at the second (unstimulated) cell. The addition of Dll4 on both cells, however, leads to higher Hes1 levels in the first cell under normoxia, a behavior that is reversed under hypoxia. Additionally, the 1 h simulations indicate that hypoxia, DAPT, and siERK1/2 addition leads to higher levels of VEGFR2 in the first cell, compared to the second cell. Dll4 stimulation, however, causes similar levels of VEGFR2 in both interacting cells, regardless of oxygen levels. In all cases, hypoxia depletes VEGFR2 levels when compared to the normoxia equivalent condition.

For a 12 h analysis, the simulation of hypoxia alone or combined with DAPT or siERK1/2 stimulation report increased Hes1 in the first cell compared to the second cell. Dll4 stimulation of both cells presents a reduced difference in the amount of Hes1 between the two cells, in both hypoxia and normoxia. Comparing the hypoxia simulations, the model shows that for 12h simulation, direct Dll4 stimulation leads to the biggest difference between the amount of Dll4 between the two cells. Under 12 h of hypoxia, the greatest difference between the amount of VEGFR2 in the two cells is noted for siERK1/2 stimulation, with the second cell presenting higher levels than the first cell.

Finally, at 24 h of stimulation, our simulations show hypoxia predominantly leading to the second cell assuming the tip cell characteristics (higher Dll4 and VEGFR2, and lower Hes1), regardless of stimulation with DAPT, siERK1/2 or Dll4, in the simulated concentrations. Endothelial cell-fate determination by the Notch signaling pathway is crucial for angiogenesis and homeostasis of the microvasculature. The simulations reported in this section provide insights into potential methods for controlling cell patterns in a system of interacting cells. Our results show the importance of considering not only the method used for interfering with the signaling pathway but also the oxygen concentration condition and the period under hypoxia for cells cultured in vitro.

4.8. eNOS phosphorylation can be modulated by Dll4, DAPT, and siERK1/2

The calcium cycling module implemented in our model is based on the previous model of Bazzazi et al. (2017). In this model, we implement a reaction representing a hypoxia-induced increase in calcium concentration through a sodium-calcium Na+ − Ca2+ exchanger. Different mechanisms are involved in calcium cycling in an endothelial cell, from the endoplasmic reticulum to the cytosol, to the extracellular environment.

Under hypoxia, intracellular calcium concentration increases, as shown by Arnould et al. (1992). Human EC subject to a period of 2 hours under hypoxia presented an increase of about 600% in cytosol calcium concentration. The increase was also reported by Berna et al. (2002), who propose that a hypoxia-induced increase in calcium levels is caused by a Na^{+} − Ca^{2+} exchanger. In the model presented, calcium signaling leads to eNOS phosphorylation, an event that biologically affects nitric oxide (NO) availability. Figure 11 shows the time courses for downstream signals, including eNOS phosphorylation under normoxia and hypoxia (1% O_2), for the stimulated and unstimulated cells.

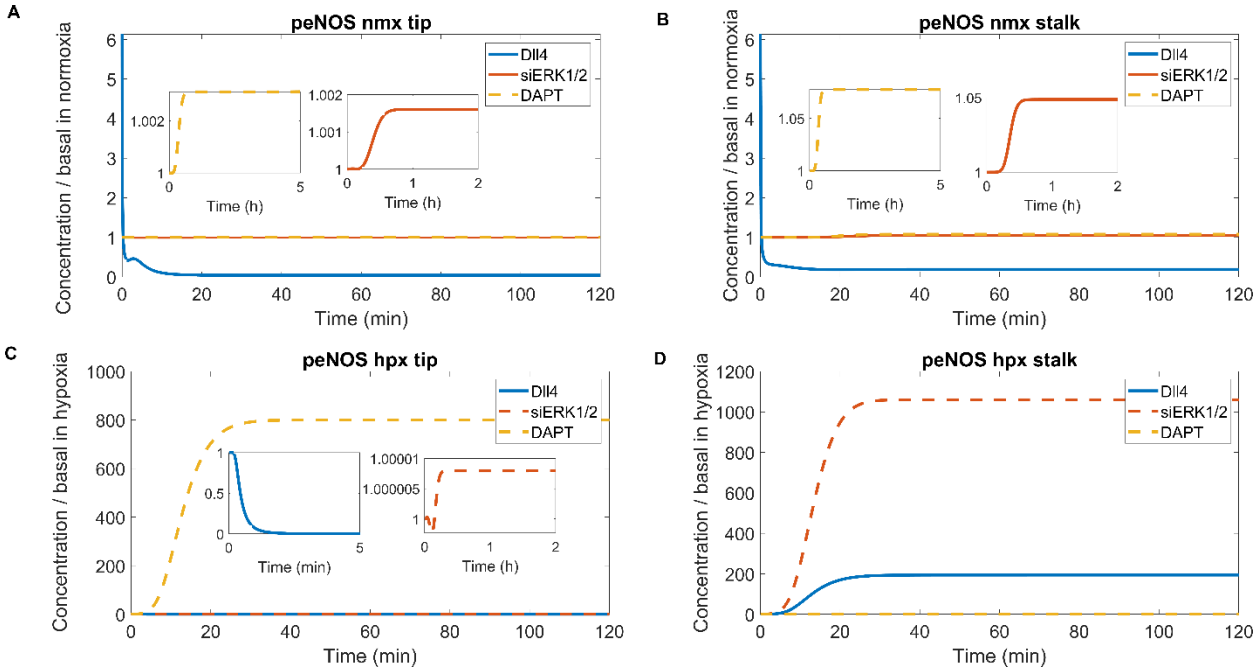

Figure 11. eNOS phosphorylation is affected by Dll4, DAPT, and siERK1/2 differently in both cells. Time dynamics of phosphorylated eNOS during normoxia in (A) the more stimulated cell. (B) the less stimulated cell; and under hypoxia (1% O_2) for the (C) more stimulated cell or the (D) less stimulated cell. hpx: hypoxia. nmx: normoxia. tip: model cell stimulated with 0.0012µM of VEGFA. stalk: model cell stimulated with 0.0006µM of VEGFA.

Our simulation shows a higher eNOS phosphorylation in tip EC than in stalk EC, which corroborates with data from Priya et al. (2015) considering that the first cell receives more VEGFA stimulation. The increase in peNOS corresponds to an increase in NO production, which guides EC sprouting. peNOS phosphorylation depends on the amount of Caveolin-1 that co-localizes with eNOS. Caveolin-1 binding to eNOS is higher in stalk cells compared with tip cells, which leads to

751 higher phosphorylation of eNOS in tip cells (Priya et al., 2015). The concentration of Caveolin-1
752 has been shown to be downregulated given growth factors stimulation (Liu et al., 2002);
753 therefore, in the model, we speculate that this relation is the major regulator of different eNOS
754 phosphorylation in the tip and stalk ECs, representing the relation through a reaction of
755 production of Caveolin which depends on VEGF concentration.

756 In addition, we observe the effects of Dll4, siERK1/2, and DAPT on eNOS phosphorylation
757 under normoxia and hypoxia for both interacting cells. Concomitant stimulation of the cells with
758 Dll4 leads to a decrease in the number of peNOS, compared to the basal peNOS under normoxia
759 levels in both cells (panels A and B). Under hypoxia, while Dll4 stimulation relates to a decrease
760 in peNOS in the tip cell, it relates to an increase in peNOS in the stalk cell (panel D). Under
761 normoxia, siERK1/2 and DAPT show little effect on altering the level of peNOS. Under hypoxia,
762 DAPT stimulation of both cells leads to an increase in peNOS relative to the normoxia peNOS
763 levels in the tip cell (panel C). Additionally, under hypoxia, the amount of peNOS relative to
764 hypoxia peNOS in the stalk cell is upregulated by siERK1/2 (panel D).

765 In summary, our simulations show an increase in eNOS phosphorylation under hypoxia
766 for both cells, during a 2 h simulation. Under hypoxia, during the initial 30 min of simulation, we
767 see a considerable increase in phosphorylated eNOS at the first cell given DAPT stimulation,
768 showing a relation between eNOS phosphorylation and the Notch signaling pathway. Also under
769 hypoxia, our simulations indicate that siERK1/2 and Dll4 lead to increases in eNOS
770 phosphorylation on the second cell, not as evident for DAPT stimulation. Therefore, the model
771 indicates that the stimulation of VEGFA, as well as the interaction through Notch, affects eNOS
772 phosphorylation and cell sensitivity to Dll4, siERK1/2, and DAPT. Such effects are not as evident
773 under normoxia.

774

775 5. Discussion

776

777 Sprouting angiogenesis as a response to hypoxia is a necessary process tightly regulated by an
778 amalgamate of agents and signaling pathways (Zhang et al., 2021; Rodriguez et al., 2021; Naito
779 et al., 2020; Hashimoto and Shibasaki, 2015). Endothelial cell patterning into the tip or stalk
780 phenotypes guide branch formation, promoting blood flow restoration to hypoxia tissues, such
781 as seen in the context of diseases like PAD (Gustafsson et al., 2005; Han et al., 2022; Annex and
782 Cooke, 2021; Kang et al., 2022). Efforts to characterize, understand, predict, and control cell
783 behavior under abnormal conditions are relevant in this field, as they can help develop new
784 therapeutic strategies and interventions.

785 In this study, we have designed a kinetics-based model of the interaction and patterning
786 of two endothelial cells stimulated with VEGFA under hypoxia and normoxia conditions. Our
787 primary goal was to investigate the differential signaling and response of each of the two cells,

788 as they are differently stimulated by VEGFA and interact through Notch signaling under hypoxia.
789 We calibrated the model using data from experiments performed in endothelial cells for both
790 oxygen conditions and defined a ratio for tip/stalk pattern identification based on known ligands
791 and receptors overexpressed in each of these phenotypes (Xu and Li, 2022; del Toro et al., 2010).
792 Considering recent efforts on designing and characterizing "virtual cells" (Zhao et al., 2019; Lim
793 et al., 2022; Zhang et al., 2021), we believe this work contributes to the field by bringing insights
794 into cell-cell interaction, patterning, and signaling with the potential translation of results to
795 pathological conditions (specifically, hypoxia-characterized diseases such as PAD).

796 As new experimental results become available, revisiting previous assumptions and
797 models is essential, making adjustments that bring us closer to natural conditions. Endothelial
798 cell patterning and interaction is a significant field of study in therapeutic angiogenesis since
799 these cells are important determinants of angiogenesis and blood flow restoration (Lim et al.,
800 2022; Qiu and Hirschi, 2019). Considering the many aspects that influence their heterogeneity
801 (Gifre-Renom et al., 2022), a computational approach provides the flexibility required to
802 implement further changes and test hypotheses. Our model reproduces characteristic EC
803 patterning behavior (Figure 6) and indicates a prolonged expression of NICD and Hes1 during
804 hypoxia compared to normoxia conditions. This is supported by previous studies showing that
805 hypoxia regulates and promotes tip/stalk differentiation through overexpression of Dll4, indirect
806 regulation of VEGFR2 and NRP1 established by Notch signaling, and upregulation of Hes1
807 (Rodriguez et al., 2021; Carmeliet et al., 2009).

808 Tip and stalk endothelial cells interact and respond differently to signals, highlighting the
809 therapeutic potential of tip-stalk cell control and selection (Chen et al., 2019). Through global
810 sensitivity analysis (Figure 5), our model allowed us to investigate this distinct behavior in a
811 system of two interacting cells, focusing on which parameters and reactions are more influential
812 in defining each cell's pattern. While we found consistency in the most significant parameters
813 and reactions between the two cells, we also noticed a distinct influence of the degradation rate
814 of internalized phosphorylated VEGFR2 on the two cells at one hour of simulation, which was not
815 seen at two hours. This indicates a time-dependency of ECPI that might lead to contrasting results
816 for more extended periods under hypoxia. Additionally, reactions related to the Akt pathway
817 were among the primary influencers of the stalk cell ECPI but not to the tip cell. As tip cells are
818 generally responsible for sensing the environment, guiding branch formation, and promoting
819 movement, while stalk cells proliferate and form lumens, following tip cells, controlling the
820 predominant phenotype might prove beneficial therapeutically (Venkatraman et al., 2016; Chen
821 et al., 2019).

822 In hypoxic PAD environments, inhibition or stimulation of the Notch signaling pathway
823 has promoted cell patterning with context-dependent benefits for improvements in ulcer healing
824 and re-establishing homeostasis and blood flow (Cao et al., 2010, 2009; Cristofaro et al., 2013;
825 Machado et al., 2019; Niu et al., 2022). Therefore, in-depth consolidation of our knowledge and
826 understanding of the interaction between endothelial cells under hypoxia conditions is necessary

827 to achieve better treatments. PAD is generally classified as a claudication or an ischemic
828 condition, and oxygen availability in the tissue is more affected in the latter. Here, we evaluated
829 different oxygen concentration levels to investigate how signaling is affected. In accordance with
830 experimental observations, we report variations in cell signaling under hypoxia and normoxia, as
831 well as between the two interacting cells under hypoxia. We also investigated the effect of
832 different hypoxia levels, noting system dependence on oxygen availability (Figure 7) and time
833 under hypoxia (Figure 8). Finally, we evaluated how our virtual cells would respond to DAPT (as
834 a direct inhibitor of the Notch pathway), siERK1/2 (as an indirect inhibitor of the Notch pathway),
835 and Dll4 (as an inducer of the Notch pathway) under normoxia and hypoxia. Once again, our
836 results indicated the difference in behavior between the interacting cells on a time-dependent
837 basis, but with potential stimulation of cell patterning through external stimuli. DAPT is
838 commonly used as a $\gamma_{\text{secretase}}$ inhibitor in vitro and in vivo, but not in human trials. Potential
839 inhibitors of this enzyme already approved for usage in clinical trials by the FDA are Nirogacestad
840 (approved for treating desmoid tumors and deep fibromatosis) and Dihydroergocristine (DHEC),
841 a drug component recently proposed for treating Alzheimer's (Kasper et al., 2022; Lei et al.,
842 2015). Future studies should focus on modeling and evaluating the pharmacokinetics and effect
843 of these inhibitors in the context of ischemia and PAD.

844 Despite our efforts to calibrate the model with experimental data from the same line of
845 endothelial cells, we were not always able to find the required data considering the level of detail
846 and ramifications of our model. Data from different cell lines might produce inaccurate
847 simulations and results (Chi et al., 2003). Another limitation of our model is not including Jagged
848 in the Notch signaling pathway, which should be accounted for in future studies, along with a
849 more detailed model of the effects of hypoxia on the calcium signaling pathway (Berna et al.,
850 2002) and of angiopoietin on the Notch signaling pathway (Machado et al., 2019). Additional
851 experimental data suggested by the present model would further validate the model. Another
852 limitation of the model is the estimation of parameters that have not been quantified in the
853 literature or in previous models. Our simulations are constrained to the estimated values. As
854 additional experimental data become available, we can revisit this constraint and update our
855 estimates. Additionally, ECs under hypoxia act differently from ECs under hypoxia serum
856 starvation, which is a future aspect to be investigated with our modeling strategy We present
857 this work as a first step in understanding the interconnection of pathways between endothelial
858 cells during hypoxia-induced angiogenesis. We believe it expands the knowledge brought by
859 previous works in the field. Future developments in expanding the model could include the effect
860 of filopodia on the EC patterning (Zakirov et al., 2021), macrophage-endothelial cell signaling, 3D-
861 modeling of interacting cells to evaluate repercussions at the tissue level, and evaluation of
862 pharmacological agents like Nirogacestad and DHEC on angiogenesis modulation.

863

864 **Acknowledgements:**

The study was funded by NIH grants R01HL101200 (ASP, BHA), R01HL148590 (BHA), R01HL141325 (BHA) and R01CA138264 (BHA), and was supported by a Graduate Fellowship from the CAPES-Fulbright-Laspau Foundation (RO).

The authors thank Yu Zhang and Min Song for reading the manuscript and for constructive comments and suggestions.

Author contributions: Conceptualization: RO and ASP; Methodology: RO; Investigation: RO; Visualization: RO; Funding acquisition: ASP and BHA; Supervision: ASP; Writing – original draft: RO; Writing – review & editing: RO, BHA, ASP.

Competing interests: The authors declare no competing interests.

Availability of data and material: The authors confirm that the data supporting the findings of this study are available within the article and the Supplementary Material. SBML code for model generation can be found at [The code will be made public on GitHub and assigned a Digital Object Identifier by Zenodo upon acceptance].

6. References

Aday, A. W. and Matsushita, K. (2021). Epidemiology of peripheral artery disease and polyvascular disease. *Circulation research* 128, 1818–1832

Akil, A., Gutiérrez-García, A. K., Guenter, R., Rose, J. B., Beck, A. W., Chen, H., et al. (2021). Notch signaling in vascular endothelial cells, angiogenesis, and tumor progression: an update and prospective.*Frontiers in Cell and Developmental Biology* , 177

Annex, B. H. and Cooke, J. P. (2021). New directions in therapeutic angiogenesis and arteriogenesis in peripheral arterial disease. *Circulation research* 128, 1944–1957

Arnould, T., Michiels, C., Alexandre, I., and Remacle, J. (1992). Effect of hypoxia upon intracellular calcium concentration of human endothelial cells. *Journal of cellular physiology* 152, 215–221

Arpino, J.-M., Yin, H., Prescott, E. K., Staples, S. C., Nong, Z., Li, F., et al. (2021). Low-flow intussusception and metastable vegfr2 signaling launch angiogenesis in ischemic muscle. *Science advances* 7, eabg9509

Balsa-Canto, E., Alonso, A. A., & Banga, J. R. (2010). An iterative identification procedure for dynamic modeling of biochemical networks. BMC Systems Biology, 4(1), 11. https://doi.org/10.1186/1752-0509-4-11

Bartoszewska, S. and Kochan, K. (2014). Piotrowski a., kamysz w, ochocka rj, collawn jf, et al. the hypoxia-inducible mir-429 regulates hypoxia-inducible factor-1 expression in human endothelial cellsthrough a negative feedback loop. *FASEB J* 29, 1467–1479

Bazzazi, H., Isenberg, J. S., and Popel, A. S. (2017). Inhibition of vegfr2 activation and its downstream signaling to erk1/2 and calcium by thrombospondin-1 (tsp1): In silico investigation. *Frontiers in physiology* 8, 48

Bazzazi, H., Zhang, Y., Jafarnejad, M., Isenberg, J. S., Annex, B. H., and Popel, A. S. (2018). Computer simulation of tsp1 inhibition of vegf–akt–enos: An angiogenesis triple threat. *Frontiers in physiology* 9,644

Benedito, R., Roca, C., Sörensen, I., Adams, S., Gossler, A., Fruttiger, M., et al. (2009). The notch ligandsdll4 and jagged1 have opposing effects on angiogenesis. *Cell* 137, 1124–1135

Berna, N., Arnould, T., Remacle, J., and Michiels, C. (2002). Hypoxia-induced increase in intracellular calcium concentration in endothelial cells: Role of the na+-glucose cotransporter. *Journal of cellular biochemistry* 84, 115–131

Blanco, R. and Gerhardt, H. (2013). Vegf and NNotch in tip and stalk cell selection. *Cold Spring Harbor perspectives in medicine* 3, a006569

Brouet, A., Sonveaux, P., Dessy, C., Balligand, J.-L., and Feron, O. (2001). Hsp90 ensures the transitionfrom the early ca2+-dependent to the late phosphorylation-dependent activation of the endothelial nitric- oxide synthase in vascular endothelial growth factor-exposed endothelial cells. *Journal of Biological Chemistry* 276, 32663–32669

Cao, L., Arany, P. R., Kim, J., Rivera-Feliciano, J., Wang, Y.-S., He, Z., et al. (2010). Modulating notch signaling to enhance neovascularization and reperfusion in diabetic mice. *Biomaterials* 31, 9048–9056 Cao, L., Arany, P. R., Wang, Y.-S., and Mooney, D. J. (2009). Promoting angiogenesis via manipulation of vegf responsiveness with notch signaling. *Biomaterials* 30, 4085–4093

Carmeliet, P. (2005). Angiogenesis in life, disease and medicine. Nature, 438(7070), 932–936. https://doi.org/10.1038/nature04478

Carmeliet, P., De Smet, F., Loges, S., and Mazzone, M. (2009). Branching morphogenesis and antiangiogenesis candidates: tip cells lead the way. *Nature reviews Clinical oncology* 6, 315–326

Chamboredon, S., Ciais, D., Desroches-Castan, A., Savi, P., Bono, F., Feige, J.-J., et al. (2011). Hypoxia- inducible factor-1α mrna: a new target for destabilization by tristetraprolin in endothelial cells. *Molecular biology of the cell* 22, 3366–3378

Chen, W., Xia, P., Wang, H., Tu, J., Liang, X., Zhang, X., et al. (2019). The endothelial tip-stalk cellselection and shuffling during angiogenesis. *Journal of cell communication and signaling* 13, 291–301 Chi, J.-T., Chang, H. Y., Haraldsen, G., Jahnsen, F. L., Troyanskaya, O. G., Chang, D. S., et al. (2003).

Chen, S., & Imoukhuede, P. I. (2019). Multiplexing Angiogenic Receptor Quantification via Quantum Dots. Analytical Chemistry, 91(12), 7603–7612. https://doi.org/10.1021/acs.analchem.9b00238

Chi, J.-T., Chang, H. Y., Haraldsen, G., Jahnsen, F. L., Troyanskaya, O. G., Chang, D. S., Wang, Z., Rockson, S. G., van de Rijn, M., Botstein, D., & Brown, P. O. (2003). Endothelial cell diversity

940 revealed by global expression profiling. *Proceedings of the National Academy of Sciences*,
941 *100*(19), 10623–10628.
942 Chiş, O., Banga, J. R., & Balsa-Canto, E. (2011). GenSSI: a software toolbox for structural
943 identifiability analysis of biological models. Bioinformatics, 27(18), 2610–2611.
944 https://doi.org/10.1093/bioinformatics/btr431
945 Chis, O.-T., Banga, J. R., & Balsa-Canto, E. (2011). Structural Identifiability of Systems Biology
946 Models: A Critical Comparison of Methods. PLoS ONE, 6(11), e27755.
947 https://doi.org/10.1371/journal.pone.0027755
948 Couffinhal, T., Silver, M., Zheng, L. P., Kearney, M., Witzenbichler, B., & Isner, J. M. (1998).
949 Mouse model of angiogenesis. *The American Journal of Pathology*, *152*(6), 1667–1679.
950 Cristofaro, B., Shi, Y., Faria, M., Suchting, S., Leroyer, A. S., Trindade, A., et al. (2013). Dll4-
951 notch signaling determines the formation of native arterial collateral networks and arterial
952 function in mouseischemia models. *Development* 140, 1720–1729
953 Debir, B., Meaney, C., Kohandel, M., and Unlu, M. B. (2021). The role of calcium oscillations in
954 the phenotype selection in endothelial cells. *Scientific reports* 11, 1–12
955 del Toro, R., Prahst, C., Mathivet, T., Siegfried, G., Kaminker, J. S., Larrivee, B., et al. (2010).
956 Identification and functional analysis of endothelial tip cell–enriched genes. *Blood, The*
957 *Journal of the American Society of Hematology* 116, 4025–4033
958 Dong, X., Wang, Y.-S., Dou, G.-R., Hou, H.-Y., Shi, Y.-Y., Zhang, R., et al. (2011). Influence of dll4
959 viahif-1α-vegf signaling on the angiogenesis of choroidal neovascularization under hypoxic
960 conditions. *PloS one* 6, e18481
961 Eelen, G., Treps, L., Li, X., & Carmeliet, P. (2020). Basic and Therapeutic Aspects of
962 Angiogenesis Updated. Circulation Research, 127(2), 310–329.
963 https://doi.org/10.1161/CIRCRESAHA.120.316851
964 Fähling, M., Persson, A. B., Klinger, B., Benko, E., Steege, A., Kasim, M., et al. (2012). Multilevel
965 regulation of hif-1 signaling by ttp. *Molecular biology of the cell* 23, 4129–4141
966 Fearnley, G. W., Smith, G. A., Abdul-Zani, I., Yuldasheva, N., Mughal, N. A., Homer-
967 Vanniasinkam, S.,et al. (2016). Vegf-a isoforms program differential vegfr2 signal transduction,
968 trafficking and proteolysis. *Biology open* 5, 571–583
969 Fish, J. E., Cantu Gutierrez, M., Dang, L. T., Khyzha, N., Chen, Z., Veitch, S., et al. (2017).
970 Dynamic regulation of vegf-inducible genes by an erk/erg/p300 transcriptional network.
971 *Development* 144, 2428–2444
972 Mac Gabhann, F., & Popel, A. S. (2006). Targeting Neuropilin-1 to Inhibit VEGF Signaling in
973 Cancer: Comparison of Therapeutic Approaches. PLoS Computational Biology, 2(12), e180.
974 https://doi.org/10.1371/journal.pcbi.0020180
975 Gifre-Renom, L., Daems, M., Luttun, A., and Jones, E. A. (2022). Organ-specific endothelial cell
976 differentiation and impact of microenvironmental cues on endothelial heterogeneity.
977 *International Journal of Molecular Sciences* 23, 1477
978 Gustafsson, M. V., Zheng, X., Pereira, T., Gradin, K., Jin, S., Lundkvist, J., et al. (2005). Hypoxia
979 requires NNotch signaling to maintain the undifferentiated cell state. *Developmental cell* 9,

980 617–628
981 Han, J., Luo, L., Marcelina, O., Kasim, V., and Wu, S. (2022). Therapeutic angiogenesis-based
982 strategy for peripheral artery disease. *Theranostics* 12, 5015
983 Hashimoto, T. and Shibasaki, F. (2015). Hypoxia-inducible factor as an angiogenic master switch.
984 *Frontiers in pediatrics* 3, 33
985 Iadevaia, S., Lu, Y., Morales, F. C., Mills, G. B., & Ram, P. T. (2010). Identification of Optimal
986 Drug Combinations Targeting Cellular Networks: Integrating Phospho-Proteomics and
987 Computational Network Analysis. Cancer Research, 70(17), 6704–6714.
988 https://doi.org/10.1158/0008-5472.CAN-10-0460
989 Imoukhuede, P. and Popel, A. S. (2011). Quantification and cell-to-cell variation of vascular
990 endothelial growth factor receptors. *Experimental cell research* 317, 955–965
991 Izumi, N., Helker, C., Ehling, M., Behrens, A., Herzog, W., and Adams, R. H. (2012). Fbxw7
992 controls angiogenesis by regulating endothelial notch activity. *PloS one* 7, e41116
993 Jakobsson, L., Franco, C. A., Bentley, K., Collins, R. T., Ponsioen, B., Aspalter, I. M., et al. (2010).
994 Endothelial cells dynamically compete for the tip cell position during angiogenic sprouting.
995 *Nature Cell biology* 12, 943–953
996 Janaszak-Jasiecka, A., Bartoszewska, S., Kochan, K., Piotrowski, A., Kalinowski, L., Kamysz, W.,
997 et al.(2016). mir-429 regulates the transition between hypoxia-inducible factor (hif) 1a and
998 hif3a expressionin human endothelial cells. *Scientific reports* 6, 1–12
999 Jin, Y., Kaluza, D., and Jakobsson, L. (2014). Vegf, notch and tgf*β*/bmps in regulation of
1000 sprouting angiogenesis and vascular patterning. *Biochemical Society Transactions* 42,
1001 1576–1583
1002 Jögi, A., Øra, I., Nilsson, H., Lindeheim, Å., Makino, Y., Poellinger, L., et al. (2002). Hypoxia
1003 alters gene expression in human neuroblastoma cells toward an immature and neural crest-
1004 like phenotype. *Proceedings of the National Academy of Sciences* 99, 7021–7026
1005 Kang, T.-Y., Bocci, F., Nie, Q., Onuchic, J. N., and Levchenko, A. (2022). Spatial-temporal order-
1006 disorder transition in angiogenic NNotch signaling controls cell fate specification. *bioRxiv*
1007 Kasper, B., Ratan, R., Alcindor, T., Schoeffski, P., van der Graaf, W. T. A., Wilky, B. A., Riedel, R.
1008 F., Lim, A., Smith, L. M., Moody, S., Attia, S., Chawla, S. P., D'Amato, G., Federman, N., van
1009 Tine, P., van Tine, B. A., Vincenzi, B., Kummar, S., & Gounder, M. M. (2022). LBA2 DeFi: A
1010 phase III, randomized controlled trial of nirogacestat versus placebo for progressing
1011 desmoid tumors (DT). *Annals of Oncology*, *33*, S1435–S1436.
1012 https://doi.org/10.1016/j.annonc.2022.08.075
1013 Kim, T. W., Yim, S., Choi, B. J., Jang, Y., Lee, J. J., Sohn, B. H., et al. (2010). Tristetraprolin
1014 regulates the stability of hif-1*α* mrna during prolonged hypoxia. *Biochemical and biophysical*
1015 *researchcommunications* 391, 963–968
1016 Koon, Y. L., Zhang, S., Rahmat, M. B., Koh, C. G., and Chiam, K.-H. (2018). Enhanced delta-
1017 notch lateral inhibition model incorporating intracellular notch heterogeneity and tension-
1018 dependent rate of delta-notch binding that reproduces sprouting angiogenesis patterns.
1019 *Scientific reports* 8, 1–15

1020 Korbecki, J., Simińska, D., Gąssowska-Dobrowolska, M., Listos, J., Gutowska, I., Chlubek, D.,
1021 et al. (2021). Chronic and cycling hypoxia: Drivers of cancer chronic inflammation through
1022 hif-1 and nf-κb activation: A review of the molecular mechanisms. *International Journal of*
1023 *Molecular Sciences* 22, 10701
1024 Kühn, C. and Checa, S. (2019). Computational modeling to quantify the contributions of
1025 vegfr1, vegfr2, and lateral inhibition in sprouting angiogenesis. *Frontiers in physiology* 10,
1026 288
1027 Lee, H.-W., Shin, J. H., and Simons, M. (2022). Flow goes forward and cells step backward:
1028 endothelialmigration. *Experimental & Molecular Medicine* , 1–9
1029 Lei, X., Yu, J., Niu, Q., Liu, J., Fraering, P. C., & Wu, F. (2015). The FDA-approved natural product
1030 dihydroergocristine reduces the production of the Alzheimer's disease amyloid-β peptides.
1031 *Scientific Reports*, *5*(1), 16541. https://doi.org/10.1038/srep16541
1032 Ligon, T. S., Fröhlich, F., Chiş, O. T., Banga, J. R., Balsa-Canto, E., & Hasenauer, J. (2018). GenSSI
1033 2.0: multi-experiment structural identifiability analysis of SBML models. Bioinformatics,
1034 34(8), 1421–1423. https://doi.org/10.1093/bioinformatics/btx735
1035 Lim, Y. C., Cooling, M., McGlashan, S., and Long, D. S. (2022). Morphological variation in an
1036 endothelial cell population: A virtual-cell model. In *International Conference on Medical*
1037 *Image Computing and Computer-Assisted Intervention* (Springer), 105–118
1038 Liu, J., Wang, X. B., Park, D. S., and Lisanti, M. P. (2002). Caveolin-1 expression enhances
1039 endothelial capillary tubule formation. *Journal of Biological Chemistry* 277, 10661–10668
1040 Londero, L. S., Hoegh, A., Houlind, K., and Lindholt, J. (2019). Major amputation rates in
1041 patients with peripheral arterial disease aged 50 years and over in denmark during the
1042 period 1997–2014 and their relationship with demographics, risk factors, and vascular
1043 services. *European Journal of Vascular andEndovascular Surgery* 58, 729–737
1044 Machado, M. J., Boardman, R., Riu, F., Emanueli, C., Benest, A. V., and Bates, D. O. (2019).
1045 Enhanced Nbtch signaling modulates unproductive revascularization in response to nitric
1046 oxide-angiopoietin signaling in a mouse model of peripheral ischemia. *Microcirculation* 26,
1047 e12549
1048 Margadant, C. (2020). Positive and negative feedback mechanisms controlling tip/stalk cell
1049 identity duringsprouting angiogenesis. *Angiogenesis* 23, 75–77
1050 Memmott, R. M. and Dennis, P. A. (2009). Akt-dependent and-independent mechanisms of mtor
1051 regulationin cancer. *Cellular signalling* 21, 656–664
1052 Moszyńska, A., Collawn, J. F., and Bartoszewski, R. (2020). Ire1 endoribonuclease activity
1053 modulates hypoxic hif-1*α* signaling in human endothelial cells. *Biomolecules* 10, 895
1054 Motulsky, H. J. and Ransnas, L. A. (1987). Fitting curves to data using nonlinear regression: a
1055 practicaland nonmathematical review. *The FASEB journal* 1, 365–374
1056 Naito, H., Iba, T., and Takakura, N. (2020). Mechanisms of new blood-vessel formation and
1057 proliferative heterogeneity of endothelial cells. *International Immunology* 32, 295–305.
1058 doi:10.1093/intimm/dxaa008
1059 Niu, H., Gao, N., Dang, Y., Guan, Y., and Guan, J. (2022). Delivery of vegf and delta-like 4 to

synergistically regenerate capillaries and arterioles in ischemic limbs. *Acta Biomaterialia* 143, 295–309

Olszewska-Pazdrak, B., Hein, T. W., Olszewska, P., and Carney, D. H. (2009). Chronic hypoxia attenuates vegf signaling and angiogenic responses by downregulation of kdr in human endothelial cells. *American Journal of Physiology-Cell Physiology* 296, C1162–C1170

O'Brien, K. A., Murray, A. J., and Simonson, T. S. (2022). Notch signaling and cross-talk in hypoxia: a candidate pathway for high-altitude adaptation. *Life* 12, 437

Paresi, C. (2016). The mechanism of action of novel gamma-secretase modulators. https://ecommons.cornell.edu/handle/1813/64685

Patel, N. S., Li, J.-L., Generali, D., Poulsom, R., Cranston, D. W., and Harris, A. L. (2005). Up-regulationof delta-like 4 ligand in human tumor vasculature and the role of basal expression in endothelial cell function. *Cancer research* 65, 8690–8697

Pedrosa, A.-R., Trindade, A., Fernandes, A.-C., Carvalho, C., Gigante, J., Tavares, A. T., et al. (2015). Endothelial jagged1 antagonizes dll4 regulation of endothelial branching and promotes vascular maturation downstream of dll4/notch1. *Arteriosclerosis, thrombosis, and vascular biology* 35,1134–1146

Priya, M. K., Sahu, G., Soto-Pantoja, D. R., Goldy, N., Sundaresan, A. M., Jadhav, V., et al. (2015). Tipping off endothelial tubes: nitric oxide drives tip cells. *Angiogenesis* 18, 175–189

Qiu, J. and Hirschi, K. K. (2019). Endothelial cell development and its application to regenerative medicine. *Circulation research* 125, 489–501

Qutub, A. A., & Popel, A. S. (2006). A computational model of intracellular oxygen sensing by hypoxia-inducible factor HIF1α. Journal of Cell Science, 119(16), 3467–3480. https://doi.org/10.1242/jcs.03087

Qutub, A. A., & Popel, A. S. (2007). Three autocrine feedback loops determine HIF1α expression in chronic hypoxia. Biochimica et Biophysica Acta (BBA) - Molecular Cell Research, 1773(10), 1511–1525. https://doi.org/10.1016/j.bbamcr.2007.07.004

Qutub, A. A., & Popel, A. S. (2008). Reactive Oxygen Species Regulate Hypoxia-Inducible Factor 1α Differentially in Cancer and Ischemia. Molecular and Cellular Biology, 28(16), 5106–5119. https://doi.org/10.1128/MCB.00060-08

Qutub, A. A., & Popel, A. S. (2009). Elongation, proliferation & migration differentiate endothelial cell phenotypes and determine capillary sprouting. BMC Systems Biology, 3(1), 13. https://doi.org/10.1186/1752-0509-3-13

Rey Barreiro, X., & Villaverde, A. F. (2023). Benchmarking tools for a priori identifiability analysis. Bioinformatics, 39(2). https://doi.org/10.1093/bioinformatics/btad065

Renardy, M., Hult, C., Evans, S., Linderman, J. J., and Kirschner, D. E. (2019). Global sensitivity analysisof biological multiscale models. *Current opinion in biomedical engineering* 11, 109–116

Rissanen, T. T., Vajanto, I., Hiltunen, M. O., Rutanen, J., Kettunen, M. I., Niemi, M., Leppänen, P., Turunen, M. P., Markkanen, J. E., Arve, K., Alhava, E., Kauppinen, R. A., & Ylä-Herttuala, S. (2002). Expression of Vascular Endothelial Growth Factor and Vascular Endothelial Growth Factor Receptor-2 (KDR/Flk-1) in Ischemic Skeletal Muscle and Its Regeneration.

The American Journal of Pathology, *160*(4), 1393–1403. https://doi.org/10.1016/S0002-9440(10)62566-7

Rodriguez, D., Watts, D., Gaete, D., Sormendi, S., and Wielockx, B. (2021). Hypoxia pathway proteins and their impact on the blood vasculature. *International Journal of Molecular Sciences* 22, 9191

Schneider, C. A., Rasband, W. S., and Eliceiri, K. W. (2012). Nih image to imagej: 25 years of image analysis. *Nature methods* 9, 671–675

Smith, T. L., Oubaha, M., Cagnone, G., Boscher, C., Kim, J. S., El Bakkouri, Y., et al. (2022). enos controls angiogenic sprouting and retinal neovascularization through the regulation of endothelial cellpolarity. *Cellular and Molecular Life Sciences* 79, 1–18

Stepanova, D., Byrne, H. M., Maini, P. K., and Alarcón, T. (2021). A multiscale model of complex endothelial cell dynamics in early angiogenesis. *PLoS computational biology* 17, e1008055

Subramanian, A., Zakeri, P., Mousa, M., Alnaqbi, H., Alshamsi, F. Y., Bettoni, L., Damiani, E., Alsafar, H., Saeys, Y., & Carmeliet, P. (2022). Angiogenesis goes computational – The future way forward to discover new angiogenic targets? Computational and Structural Biotechnology Journal, 20, 5235–5255. https://doi.org/10.1016/j.csbj.2022.09.019

Swaminathan, B., Youn, S.-W., Naiche, L., Du, J., Villa, S. R., Metz, J. B., et al. (2022). Endothelial NNotchsignaling directly regulates the small gtpase rnd1 to facilitate notch suppression of endothelial migration. *Scientific Reports* 12, 1–14

Takeshita, K., Satoh, M., Ii, M., Silver, M., Limbourg, F. P., Mukai, Y., et al. (2007). Critical role of endothelial notch1 signaling in postnatal angiogenesis. *Circulation research* 100, 70–78

Teleanu, R. I., Chircov, C., Grumezescu, A. M., and Teleanu, D. M. (2019). Tumor angiogenesis and anti-angiogenic strategies for cancer treatment. *Journal of clinical medicine* 9, 84

Tiemeijer, L. A., Ristori, T., Stassen, O. M. J. A., Ahlberg, J. J., de Bijl, J. J. J., Chen, C. S., Bentley, K., Bouten, C. V. C., & Sahlgren, C. M. (2022). Engineered patterns of Notch ligands Jag1 and Dll4 elicit differential spatial control of endothelial sprouting. IScience, 25(5), 104306. https://doi.org/10.1016/j.isci.2022.104306

Ulyatt, C., Walker, J., and Ponnambalam, S. (2011). Hypoxia differentially regulates vegfr1 and vegfr2 levels and alters intracellular signaling and cell migration in endothelial cells. *Biochemical and biophysical research communications* 404, 774–779

Van Lessen, M., Nakayama, M., Kato, K., Kim, J. M., Kaibuchi, K., and Adams, R. H. (2015). Regulation of vascular endothelial growth factor receptor function in angiogenesis by numb and numb-like. *Arteriosclerosis, thrombosis, and vascular biology* 35, 1815–1825

Venkatraman, L., Regan, E. R., and Bentley, K. (2016). Time to decide? dynamical analysis predicts partial tip/stalk patterning states arise during angiogenesis. *PLoS One* 11, e0166489

Villa, J. C., Chiu, D., Brandes, A. H., Escorcia, F. E., Villa, C. H., Maguire, W. F., et al. (2014). Nontranscriptional role of hif-1α in activation of γ-secretase and notch signaling in breast cancer. *Cellreports* 8, 1077–1092

1139 Wang, R., Yang, Z., Liang, L., Feng, X., Che, B., Zhang, X., et al. (2022). Notch activation
1140 suppresses endothelial cell migration and sprouting via mir-223-3p targeting fbxw7. *In Vitro*
1141 *Cellular & Developmental Biology-Animal* 58, 124–135
1142 Weddell, J. C. and Imoukhuede, P. I. (2017). Integrative meta-modeling identifies endocytic
1143 vesicles, late endosome and the nucleus as the cellular compartments primarily directing rtk
1144 signaling. *Integrative Biology* 9, 464–484
1145 Weinstein, N., Mendoza, L., Gitler, I., and Klapp, J. (2017). A network model to explore the
1146 effect of themicro-environment on endothelial cell behavior during angiogenesis. *Frontiers*
1147 *in physiology* 8, 960 Winter, J. N., Jefferson, L. S., and Kimball, S. R. (2011). Erk and akt
1148 signaling pathways function through parallel mechanisms to promote mtorc1 signaling.
1149 *American Journal of Physiology-Cell Physiology* 300, C1172–C1180
1150 Xu, L. and Li, C. (2022). Network-based analysis reveals gene signature in tip cells and stalk
1151 cells. *Anti-Cancer Agents in Medicinal Chemistry (Formerly Current Medicinal Chemistry-Anti-*
1152 *Cancer Agents)* 22, 1571–1581
1153 Zakirov, B., Charalambous, G., Thuret, R., Aspalter, I. M., Van-Vuuren, K., Mead, T., Harrington,
1154 K., Regan, E. R., Herbert, S. P., & Bentley, K. (2021). Active perception during angiogenesis:
1155 filopodia speed up Notch selection of tip cells in silico and in vivo . Philosophical
1156 Transactions of the Royal Society B: Biological Sciences, 376(1821), 20190753.
1157 https://doi.org/10.1098/rstb.2019.0753
1158 Zhang, Y., Wang, H., Oliveira, R. H. M., Zhao, C., and Popel, A. S. (2021). Systems biology of
1159 angiogenesis signaling: Computational models and omics. *WIREs Mechanisms of Disease* ,
1160 e1550
1161 Zhang, Y., Zhao, C., and Popel, A. S. (2022). Chapter 14 - systems biology modeling of
1162 endothelial cell and macrophage signaling in angiogenesis in human diseases. In *The*
1163 *Vasculome*, ed. Z. S. Galis (Academic Press). 163–172. doi:https://doi.org/10.1016/B978-0-
1164 12-822546-2.00021-6
1165 Zhang, Z., Yao, L., Yang, J., Wang, Z., and Du, G. (2018). Pi3k/akt and hif-1 signaling pathway
1166 in hypoxia-ischemia. *Molecular medicine reports* 18, 3547–3554
1167 Zhao, C., Mirando, A. C., Sové, R. J., Medeiros, T. X., Annex, B. H., and Popel, A. S. (2019). A
1168 mechanistic integrative computational model of macrophage polarization: implications in
1169 human pathophysiology.*PLoS computational biology* 15, e1007468
1170 Zhao, C. and Popel, A. S. (2015). Computational model of microrna control of hif-vegf pathway:
1171 insights into the pathophysiology of ischemic vascular disease and cancer. *PLoS*
1172 *computational biology* 11, e1004612
1173

1174

1175 **Supplementary material**

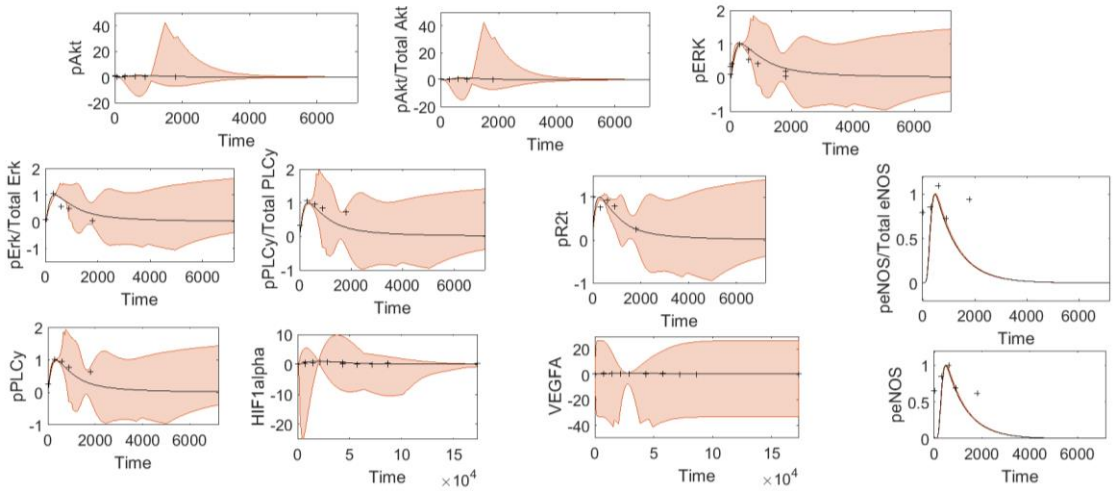

S 1: Confidence intervals post-normoxia fitting. The confidence intervals were computed post-fitting, using Gaussian 95% setting on SimBiology model analyzer.

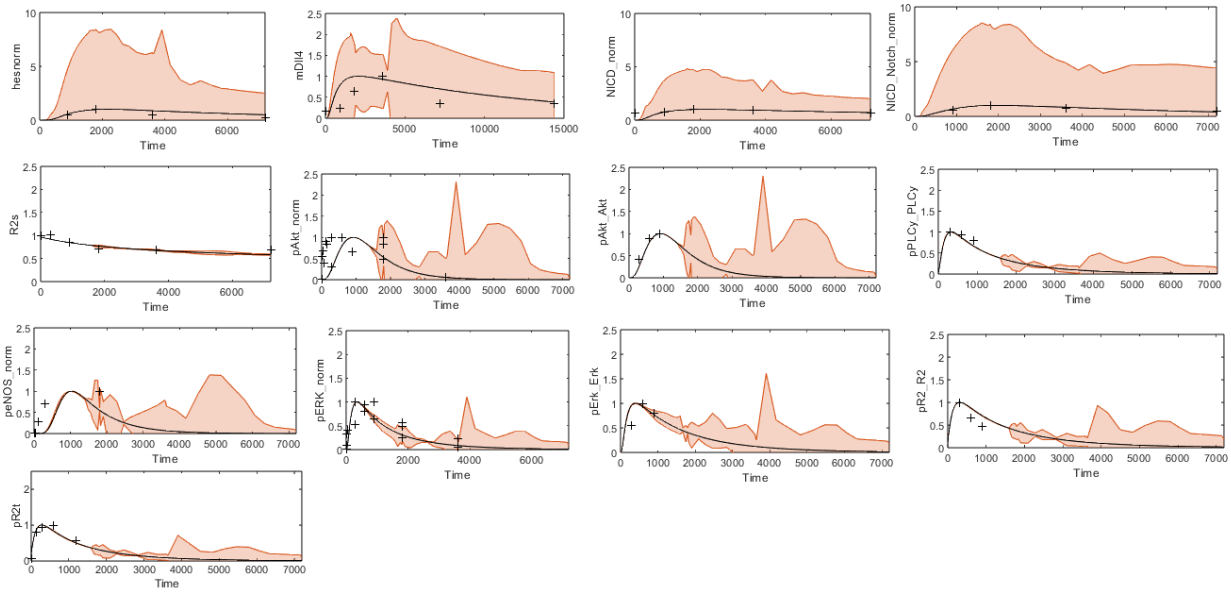

S 2: Confidence intervals post-hypoxia fitting. The confidence intervals were computed post-fitting, using Gaussian 95% setting on SimBiology model analyzer

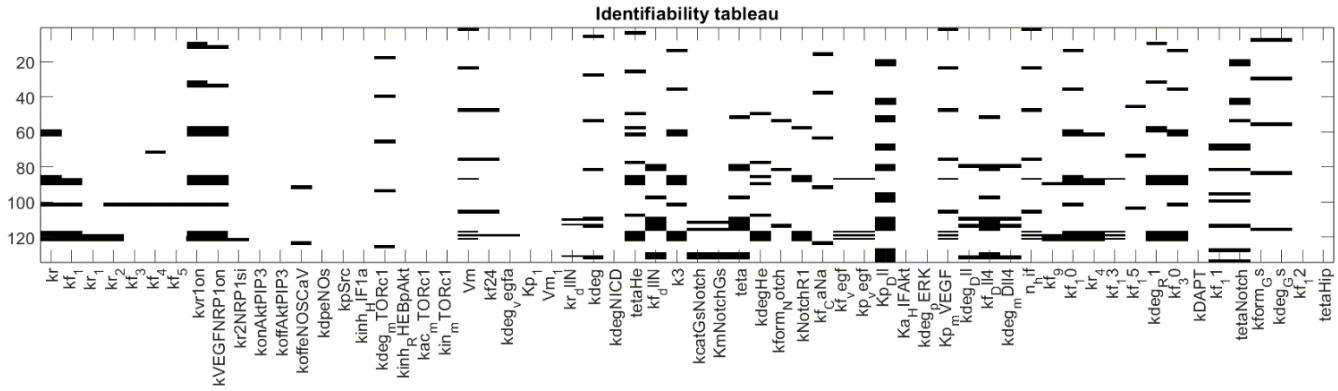

S 3: Identifiability tableau. Parameters evaluated are listed on the X-axis, and the Y-axis represents non-zero series coefficients. Empty columns represent non-identifiable parameters (Chis et al., 2011).

The following are available as an Excel file.

Table S1: PRCC and p-values

Table S2: ODEs

Table S3: Reactions

Table S4: Parameters

Table S5: Variants

Table S6: Observables

Table S7: Species

Local Sensitivity analysis of Hes1 to VEGFR2

To investigate how the initial value of receptors VEGFR2 influences cell patterning, we performed Local Sensitivity Analysis (LSA) on Hes1 in both cells using SimBiology Model Analyzer, for 7200 seconds, with the first cell being stimulated with more VEGFA (0.0012uM) than the second one (0.0006 uM). For this simulation, the initial amount of VEGFR2 in both cells is set to 0.0099 uM. This simulation was performed using the normoxia-fitted model. Our first result (Figure S4 A and B) shows the magnitude of the computed sensitivities integrated over time. The model indicates that under such conditions VEGFR2 on the second cell exerts a higher influence on Hes1 in both cells, although Hes1 in the two cells is sensitive to the initial amount of receptors in both cells.

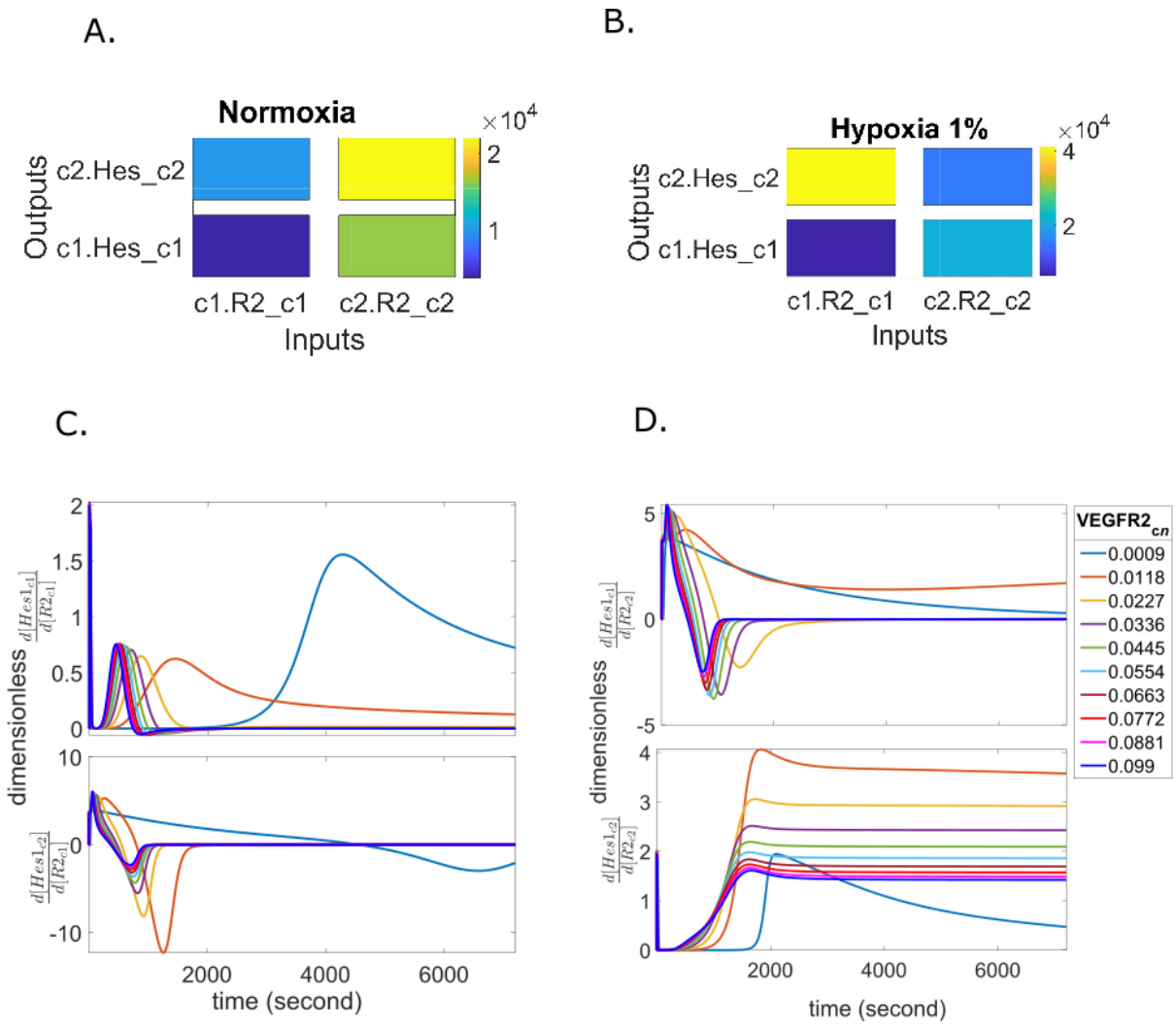

S 4: Local sensitivity analysis of Hes1 to changes in VEGFR2 in both cells. Sensitivity of Hes1 in both cells to the initial values of VEGFR2 under normoxia (A) or hypoxia (B). The effect of varying the concentration of VEGFR2 on the stimulated (C) or the unstimulated (D) cells on Hes1 sensitivity. Abbreviations: R2 = VEGFR2; n = 1 or 2; c1 = cell 1 (stimulated); c2 = cell 2 (unstimulated).

We then vary the receptor's concentration (one order of magnitude above and below 0.0099 uM) in both cells to see how this affects the sensitivity over time of Hes1 under normoxia. Figure S4 C shows the sensitivity over time of Hes1 for the first (top diagram) cell and the second (bottom diagram) cell given a variation in the initial concentration of VEGFR2 of the first cell in time. Similarly, Figure S4 D shows the change in sensitivity in time of Hes1 in both cells to VEGFR2 of the second cell. The results indicate a higher influence of the first cell receptor concentration on Hes1 sensitivity before the first 30 minutes (1800 seconds) of simulation (Figure S4 C). Increased values of VEGFR2 in the second cell lead to prolonged influence on Hes1 sensitivity in the second cell (Figure S4 D, bottom diagram) compared to increasing VEGFR2 in the first cell (Figure S4 C, bottom diagram). Our results also indicate that defining receptor concentration different than the estimated initial concentration used in this work affects Hes1 sensitivity.